

AquaHaptics: Hand-based Multimodal Haptic Interactions for Immersive Virtual Underwater Experience

Soyeong Yang and Sang Ho Yoon, *Members, IEEE*

Abstract—With the advancement of haptic interfaces, recent studies have focused on enabling detailed haptic experiences in virtual reality (VR), such as fluid-haptic interaction. However, rendering forces from fluid contact often causes a high-cost computation. Given that motion-induced fluid feedback is crucial to the overall experience, we focus on hand-perceivable forces to enhance underwater haptic sensation by achieving high-fidelity rendering while considering human perceptual capabilities. We present a new multimodal (tactile and kinesthetic) haptic rendering pipeline. Here, we employ drag and added mass forces by dynamically adapting to the user's hand movement and posture with pneumatic-based haptic gloves. We defined decaying and damping effects to indicate fluid properties caused by inertia and confirmed their significant perceptual impacts compared to using only physics-based equations in a perception study. By modulating pressure variations, we reproduced fluid smoothness via exponential tactile deflation and light fluid mass via linear kinesthetic feedback. Our pipeline enabled richer and more immersive VR underwater experiences by accounting for precise hand regions and motion diversity.

Index Terms—Human-computer interaction, Fluid-haptic Rendering, Human perception, Virtual reality.

I. INTRODUCTION

THE sense of presence has become increasingly crucial in virtual reality (VR) due to inducing users to feel like they are ‘being there’ or involved in the environment [1]–[3]. It allows users to interact or modify objects [4], [5] or receive sensory feedback remotely [6] to enhance the experience or cognitive performance. By presenting the physical presence and reducing the gap between the virtual and real worlds, various haptic interfaces and rendering algorithms have been introduced. While existing approaches have studied rigid-object interactions, fluid interaction is also crucial for a rich VR experience [7], [8]. Enabling fully interactive VR fluid environments has the potential to expand applications in education [9], exploration [10], [11], training [12]–[14], and entertainment [15]–[17]. The increased number of fluid-based VR applications has driven the development of haptic rendering algorithms that capture the dynamics of fluid-haptic interaction and convey immersive haptic sensation.

Early fluid haptic rendering research mainly addressed fluid simulation for accurate force computation. Dobashi et al. stored pre-calculated forces in a database [18]. To further

Soyeong Yang and Sang Ho Yoon are with the Human-Centered Interactive Technologies Lab, Korea Advanced Institute of Science and Technology, Daejeon, Republic of Korea (email: sy.yang@kaist.ac.kr, sangho@kaist.ac.kr)

Manuscript received April 19, 2021; revised August 16, 2021.

accelerate simulation, other studies utilized GPU processing for heavy computation [19]–[21]. However, these methods remain computationally demanding and typically restrict interactions to small fluid volumes with grounded haptic interfaces. Our research aims to render key perceivable forces without relying on full fluid simulation, thereby improving efficiency and accessibility for immersive fluid-haptic applications.

From a perceptual perspective, the primary force experienced during underwater motion acts opposite to the movement direction [22]. Several studies simulated this as a “drag force” combined with visual feedback, tracking users' hand [23] or limb motions [24] and applying visually delayed motion effects corresponding to drag magnitude. However, visual illusion alone cannot provide a rich experience. To this end, previous work [23] reported that utilizing sophisticated hardware with actual stimulus enhances the user experience in the virtual fluid environment. Building on this idea, later work reproduced the fluid resistance using an exoskeleton robot arm [25] or lower limb brakes [26], focusing particularly on drag force. Instead of the high-cost fluid simulation, they showed that implementing perceptible fluid forces has a meaningful impact even with simplified fluid dynamics. Schmidt et al. further suggested that increasing tactile interface points beyond the robot's three haptic contacts would enable more complex perception of the virtual environment [25]. These findings motivate us to explore improved fluid sensation through multi-point and multimodal haptic interfaces.

When humans move their limbs underwater, drag force and added mass force occur based on their movements [27]. Here, the drag force acts normal to the hand surface, and the added mass force arises according to the hand acceleration [28]. To the best of our knowledge, there is no standard method to render fluid resistance while reflecting hand-specific elements. Rather than conducting intensive fluid simulations for precise force rendering, we focused on rendering two perceptually dominant forces (drag and added mass forces) on the hand to balance between physics fidelity and perceptual performance.

We present a multimodal haptic rendering pipeline that replicates real-water properties by reflecting hand movement and posture. The proposed pipeline employs wearable pneumatic-based haptic gloves (DK2, HaptX Inc.¹). The gloves support tactile feedback through an inflatable pneumatic bubble called a ‘tactor’ and kinesthetic feedback via a passive wire-driven brake called a ‘retractuator’. To deliver high-

¹<https://haptx.com/>

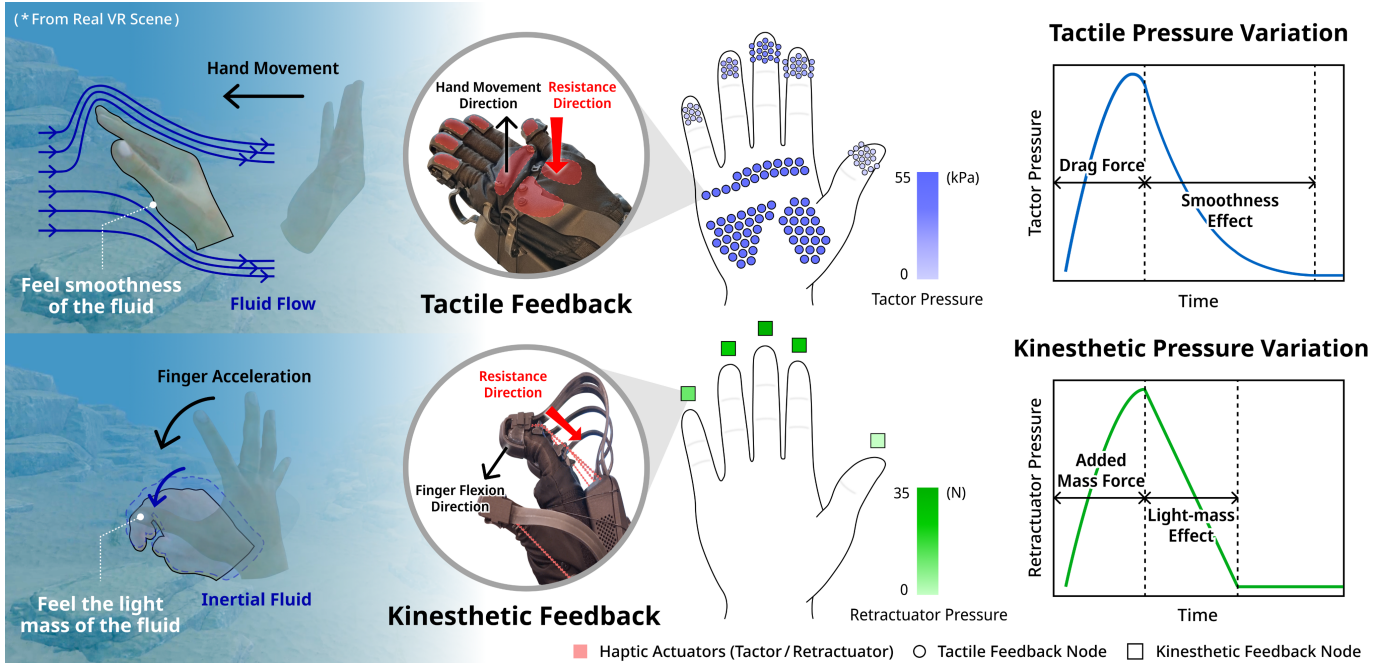


Fig. 1. Overview of the proposed hand-based haptic interaction pipeline in a fluid-filled VR environment. We provide multimodal haptic feedback incorporating drag and added mass forces, which are cognitively influential for the immersive experience in virtual underwater settings. Based on the hand movement or individual finger's posture, the system dynamically adjusts actuator activation, rendering regions, pressure variations, and durations to improve realism.

fidelity feedback, we defined movement-reflected and posture-reflected elements and rendered the forces corresponding to each tactile and kinesthetic actuator. By designing fluid parameters to generate realistic variations in fluid pressure and a continuous flowing sensation on the hand, we explored optimal force mappings through user studies. Most participants preferred tactile feedback that decayed exponentially to enhance the smoothness of the fluid, and kinesthetic feedback with linear damping to represent the light mass of the fluid.

We conducted an application study with an underwater swimming scenario employing the proposed pipeline in both hands. Compared to the condition using uniform tactile and kinesthetic feedback, our method, incorporating hand movement- and posture-reflected elements, enhanced overall user experience across perceptual and subjective dimensions.

Hence, our main contributions are as follows:

- A real-time fluid haptic rendering pipeline enabling hand interactions with drag and added mass forces to achieve both physical fidelity and perceptual performance;
- A multimodal rendering design integrating tactile and kinesthetic feedback based on hand movements and postures in the underwater environment;
- Perceptual analysis establishing design guidelines for realistic haptic sensations and defining fluid properties for immersive VR fluid experience; and
- A rich haptic experience in the underwater VR environment reflecting the hand-specific elements.

II. RELATED WORK

A. Haptic Rendering for Fluid

To enhance user experiences with fluid media, researchers have explored which fluid-induced forces should occur during

user interaction. An early study divided fluid dynamics into linear and precomputed non-linear flows using the Navier-Stokes equations [18], introducing a fluid resistance map that computes buoyancy, frictional, and pressure resistances in advance for storage. To address resource and stability issues, a deformable grid-based fluid simulation approach was proposed [29], [30]. Although this method enables real-time computation, it requires a fixed cell size and may generate pressure artifacts at cell boundaries, limiting its applicability to haptic interactions.

To render forces within particle-based fluids, haptic rendering has mainly focused on intuitive interactions between rigid-fluid (haptic proxy-fluid particle). For realistic simulations with complex physical properties, smoothed particle hydrodynamics (SPH) has been widely used to model pressure and viscosity forces with deformable material on GPUs [31]. Hybrid approaches combining SPH fluids with flexible, discretized proxies have also been introduced to compute pressure, viscosity, and external forces. Several studies have further addressed buoyancy effects in underwater or confined environments. For example, Liang et al. simulated buoyancy and drag forces using SPH [32], while Cheng et al. developed a multisensory system integrating haptic and auditory feedback for pressure, viscosity, and buoyancy [33]. These works highlight the importance of pressure and drag forces in counteracting probe motion within a fluid medium. However, implementing a large scale of particle–rigid interactions on GPUs remains computationally expensive [34], [35].

Recent studies have therefore aimed to reduce the computational cost of fluid simulation and render the primary resistance forces that greatly affect human perception. For example, drag-based viscous fluid rendering using a hand-arm

exoskeleton [25], a limb exoskeleton [26] has been employed to deliver sensations of fluid resistance. This method could provide sufficient realism for users, even with simplified fluid dynamics. Furthermore, the author [26] mentioned that rendering the added mass force based on limb acceleration could further enhance the realism of virtual underwater interactions. We adopted this approach by focusing on the most influential forces in underwater environments where human hands move dynamically. To the best of our knowledge, no prior work has addressed haptic feedback rendering of both drag and added mass forces in an underwater environment.

B. Haptic Interface for Fluid Interaction

There are multiple use cases of haptic interfaces for force, tactile, and multimodal feedback rendering for fluid interaction. During the last decade, stylus-type haptic devices that provide force feedback have been mainly used. The haptic proxy interface was employed in some studies to calculate contact forces with fluid particles [22], [36], while others computed both forces and torques produced between the proxy's position and the fluid particle or external sources during fluid exploration [19], [30], [37]. However, this stylus-based force feedback approach cannot convey detailed sensations when interacting with diverse probes in a fluid-filled environment.

Studies have also developed hardware that delivers more realistic physical feedback using actuators over large areas for tactile rendering. Mid-air haptics offers precision control and high-frequency tactile feedback by generating ultrasound waves at specific locations [21], [38], [39]. It can reproduce falling water sensations on the hand through fluid simulation focused on pressure distribution. Nevertheless, such devices are typically grounded or unattached and cannot restrict user motion caused by resistive forces in three dimensions.

More recently, haptic rendering methods providing multimodal feedback have been explored. Liu et al. developed liquid bladders with vibration actuators wrapping hands by rendering various sensations such as pressure, vibration, and temperature of the water [40]. Their results suggested that multimodal feedback matched with the user's movement could improve the realism. However, few algorithms currently support various modalities with a single device for fluid-haptic interaction. To compensate for this limitation, we propose a novel fluid interaction pipeline that combines tactile and kinesthetic actuation with high degrees of freedom to allow free-hand motion.

C. Body-specific Haptic Rendering

Many rendering methods modulate the intensity or direction of haptic feedback according to the user's body location, motion, or posture to enhance perception.

T-hive, for instance, is a sphere-shaped handle interface that provides spatial sensations via vibrotactile feedback [41]. It shows six degrees-of-freedom (6-DoF) bilateral information and logarithmic decaying intensity on the surface where the user's palm is grasping. Using pattern or recognition cues has also proved that vibrotactile patterns on the forearm or torso are effective [42]. Some studies have generated lateral motion on the forearm [43], [44] using linear arrays of vibrotactile

motors or pneumatic actuators [45] by creating sequential peaks of intensity. It has been demonstrated that providing only pressure without vibration has a continuity effect as well. Even sparse 2D tactile actuators on the palm can deliver continuous tactile strokes when adjacent tactors overlap [44], [46].

In terms of force feedback, Airpush indicates a total of eight horizontal and vertical directions on fingertips using compressed air [47]. This wearable haptic device can render five different moduli of elastic sensation and fluid resistance within the stream. Jo et al. made their own wearable haptic gloves and provided the linearly decreasing force feedback as the fingertip moves from the surface toward the center of a soft object [48]. Inspired by these studies, we extended the concept to represent water flow sensations on the human hand by giving directional pneumatic feedback.

Although various body-specific feedback rendering algorithms exist for different body parts, fluid-interaction systems that incorporate the hand-specific elements are insufficient. In this study, we confirmed the effectiveness of pressure-based pneumatic tactile feedback that provides flow sensations on the palm, as well as kinesthetic feedback synchronized with finger movements to represent fluid properties.

III. AQUAHAFTICS OPERATING PRINCIPLE

A. Virtual Underwater Configuration

In this work, we set two assumptions for virtual fluid dynamics, which include 1) static fluid and 2) turbulent flow.

Assumption 1. Static Fluid: We consider a virtual underwater composed of stationary fluid, with only the user's hand moving. When the hand stops, the fluid is considered not to be moving. This condition aligns with previous fluid simulation studies [49], [50]. Alternatively, it can be interpreted as the hand remaining fixed while the fluid moves toward it.

Assumption 2. Turbulent flow: Artificial paddling with the hand generally produces a high Reynolds number ($Re > 10^4$) [51], where the dominant hydrodynamic forces are pressure drag and added mass forces. Even in a stationary fluid, rapid acceleration or high-speed hand motion induces boundary layer instabilities that lead to turbulence.

In fluid dynamics, the drag force consists of two primary components: pressure drag and friction drag. The pressure drag arises from the pressure difference between the object and the surrounding fluid, whereas friction drag results from viscous friction along the object's surface. We assume that the fluid flow approaches the hand perpendicularly in a high Reynolds number regime. Then, the pressure drag dominates and the effect of friction drag becomes negligible [52]. If friction drag were significant, it would act tangentially along the hand surface according to $F = 6\pi\eta rv$, where F is friction drag, η is the fluid viscosity, r is the object radius, and v is the object's velocity. Accordingly, we did not take into account the frictional resistance, hand roughness, and viscosity force. We also excluded wake effects [53], as turbulent flow promotes boundary-layer separation farther downstream of the hand surface compared to laminar flow [54].

$$F = F_D + F_M. \quad (1)$$

In Eq. 1, F is the overall rendering force applying to the whole hand, F_D represents the drag force, and F_M is the added mass force. As mentioned earlier, we rendered the drag force using pneumatic tactors for tactile feedback and the added mass force using retractuators for kinesthetic feedback. The tactile feedback is applied normally toward the palm, while the kinesthetic feedback pulls the finger from the back of the hand, following prior work [55]. We enable localized penetrating forces across the entire hand by integrating these haptic rendering methods.

1) *Drag Force*: The drag force generally acts on the object's surface. We generated a drag force sensation on the palm by controlling tactor inflation to simulate localized fluid pressure based on Eq. 2.

$$F_D = \frac{1}{2} \rho (v')^2 C_D A, \quad (2)$$

$$v' = v \cos \theta. \quad (3)$$

In Eq. 2, ρ denotes the water density ($\approx 998.6 \text{ kg/m}^3$ at 18°C), and v' is the relative velocity between the water flow and the hand. In detail, the drag force acts in the normal direction on the object's surface [56], opposing the local orientation of inclined palm regions or bent fingers. Therefore, we multiplied the cosine of the tilt angle ($\theta, 0^\circ \leq \theta \leq 90^\circ$) with v [57], [58], the pure opposite velocity of the human hand (Eq. 3). C_D is the drag coefficient depending on the object's shape, and A is the projected cross-sectional area against the flow.

Using pneumatic tactors on the palm to provide physical feedback, we determined C_D and A from tactor specifications. When the hand moves normally, we set C_D as 0.42 for a hemisphere-shaped tactor [59], [60]. We used different tactor sizes for palm (6.1 mm) and finger (4.5 mm) to compute A , yielding $9.3025 \times 10^{-6} \text{ m}^2$ and $5.0625 \times 10^{-6} \text{ m}^2$.

In the case of lateral hand movements, the first contact part of the hand with the fluid is the side of the hand. From a simple point of view, we regarded the side as a rectangular cylinder to decide the object's coefficients from the neutral hand state. Even though there are no tactors on the hand's side, forces were computed using C_D as 1 [61] and A as 0.0028 m^2 [62] based on the shape of the hand's side. Prior work shows C_D remains consistent within the range of 0.50 to 0.56 when there is a hand rotation [63]. Since the hand size is so small relative to the whole underwater environment, this variation introduces negligible error in total drag estimation.

2) *Added Mass Force*: From the perspective of fluid simulation, previous works [22], [29] used a spring-damper system with a haptic probe to simulate the probe's deceleration caused by fluid resistance. The haptic probe, a handle-type interface, enables single-point interactions with virtual objects when held by the user. This probe usually renders the reaction force when entering or moving within the fluid.

Since our setup does not include a physical spring connected to the haptic probe, we applied the inertia force equation accounting for added mass [28]. As weight-related sensation is mainly perceived through force feedback [64], we used retractuators to deliver force from fluid inertia. We modeled

the human finger instead of a haptic probe, as users directly control their fingertip as the end-effector. When the finger bends with acceleration in a virtual underwater environment, its movement is constrained by the inertia of the surrounding fluid mass. The added mass force is defined in Eq. 4.

$$\begin{aligned} F_M &= (m + m_{\text{added}})a \\ &= (\rho_{\text{object}} V + \rho_{\text{water}} C_M V)a. \end{aligned} \quad (4)$$

Here, m and m_{added} are the object's intrinsic mass and underwater added mass, respectively. Each ρ_{object} and ρ_{water} denotes the density of the object (in this case, a finger, $\approx 1,050 \text{ kg/m}^3$) and water. C_M is an added-mass coefficient depending on the object's shape. For a simplified cylinder-shaped finger, we set C_m to 1 [65]. V is the object's volume, and a its acceleration. The acceleration ($a = v \cdot \frac{\Delta v}{\Delta t}$) of the finger was derived from the position of the distal interphalangeal (DIP) joint. Based on the distal phalanges, we designated $(m + m_{\text{added}})$ of thumb, index, middle, ring, and pinky as $2.4 \times 10^{-6} \text{ kg}$, $2.4 \times 10^{-6} \text{ kg}$, $2.7 \times 10^{-6} \text{ kg}$, $2.2 \times 10^{-6} \text{ kg}$, and $1.4 \times 10^{-6} \text{ kg}$, individually [62].

B. Underwater Interaction Design

1) *Movement-reflected Elements*: we classified hand movement directions to identify the fluid-facing side before rendering fluid interaction. We ensure a consistent movement direction based on the displacement of the palm center, regardless of wrist rotation.

a) *Directional Vector*: To provide a sensation of fluid pressure during fluid-hand interaction, we first specified the initial rendering location on the hand. We define the center of the palm as the midpoint between the metacarpophalangeal joint (MCP) of the index, MCP of the pinky, and the wrist [66]. From this center point, we established six directional vectors (Fig. 2 (a)) representing possible hand movement directions. Here, we assumed that the water flow approaches from the opposite direction of the hand movement and extended several vectors from the limited hand motions (diving up, down, and forward) in previous work [40].

Considering human ergonomics, the wrist tends to follow a straight trajectory during horizontal arm movements [67]. The resulting movement exhibits a nearly linear tangential velocity profile, maintaining consistency even when the trajectory is slightly curved [68]. As shown in Fig. 2 (b), we suggest six directional vectors originating from a human hand. When a person moves their arm normally or laterally, they can perceive the fluid flowing across the palm in an orthogonal direction.

b) *Haptic Rendering Region*: To enable realistic fluid sensation during lateral hand movements, we introduce numerous haptic rendering regions across the hand in Fig. 3 (b). With regard to the normal motion, we divided the hand's area into regions based on skin-foldable parts [69]. This includes the palm into three parts (palmar, hypothenar, and thenar) and five fingertip areas. Within an identical rendering region, the exerted force is the same due to having the same velocity (v).

For lateral motion, the side of the hand initially interacts with the fluid. However, tactors exist only on the palm side, with none on the lateral side, as shown in Fig. 3 (a). To address

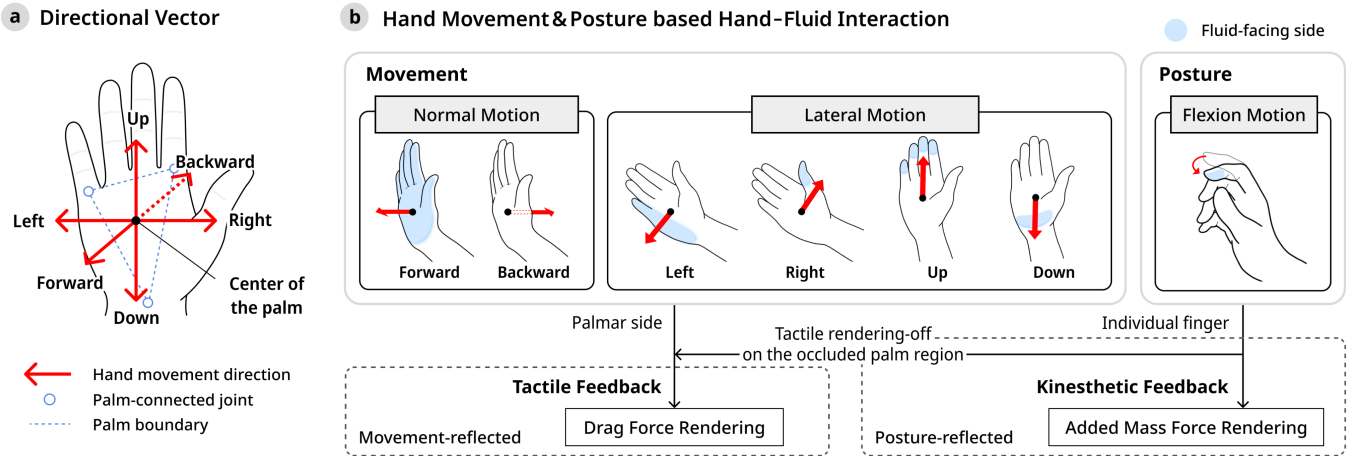


Fig. 2. AquaHaptics working principle and system overview. (a) Definition of directional vectors for hand movements. (b) The hand-fluid interaction hierarchy according to the hand movement or posture.

this limitation, we induce a tactile illusion by sequentially activating tactors in lateral order to enhance the flow sensation. Hence, lateral boundaries are divided into five parts for all lateral directions (Fig. 3 (b)). Due to the tactor configuration on the glove, we cannot adjust all individual tactors but control tactors sharing the same pneumatic hose instead. Based on the two-point discrimination threshold of about 10 mm on the human palm [70], we fixed the size of each lateral boundary to match the tactor arrangement. Tactors in the outermost boundary, which are directed opposite to the directional vector, are rendered first, allowing users to perceive the fluid flow as a continuous sequence of localized sensations [71].

c) *Overlap Ratio*: To induce the sensation of lateral fluid flow using only normally pressing tactors, we employed a sequential activation method that evokes the perception of continuous transverse motion [45]. Similar to previous work, we generated the overlap ratio between two consecutive lateral rendering regions to increase the natural sensation of fluid flowing by pneumatic actuators.

d) *Decaying Effect*: When the user suddenly stops their hand in the fluid, the perceived pressure on the palm rapidly increases and then gradually decreases as surrounding fluid accumulates around the hand [73]. Since we assumed a static fluid condition, the fluid pressure decreases as the hand pauses, disregarding any wake flow. Moreover, we suggest the concept of pressure variation shown in Fig. 4 (a), which characterizes the decaying and duration of fluid pressure for more natural fluid-haptic feedback [22]. We utilized *decaying effect* on the palmar side of the hand to implement the pressure variation.

The rendering force is determined by the pre-computed drag force based on the hand movement. When the user changes hand posture through finger flexion, the drag force is exerted on the palmar side of the fingertip, and an additional added-mass force is provided through kinesthetic feedback.

2) *Posture-reflected Elements*: Different from the neutral state of the hand with all fingers extended, finger flexion changes the overall hand posture. As the posture changes, users experience kinesthetic feedback on the dorsal side of their hand, perceiving the inertia of the surrounding fluid mass.

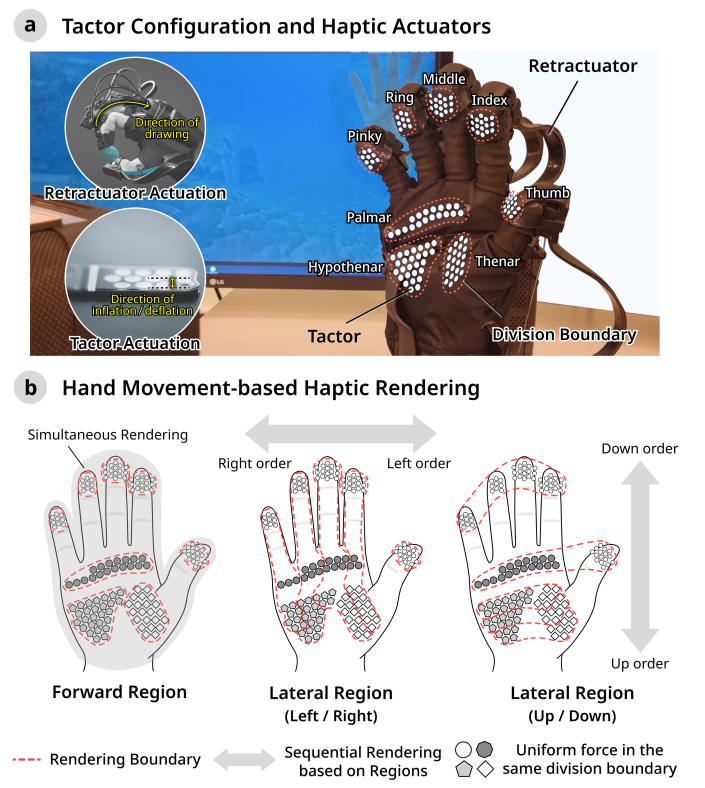


Fig. 3. Hardware specifications and rendering mechanism. (a) Haptic glove configuration of all pneumatic tactors and retractors. The actuation footages are from HaptX [72]. (b) We define haptic rendering regions based on hand movement type. When the hand moves left-right or up-down, the activation order of rendering region is opposite to the direction of hand movement.

Some areas of the palm and fingertips may not be in contact with fluid, so we define these as occluded regions on the palm.

a) *Sustained & Damping Effect*: Instead of using a conventional spring-damper model for force feedback, we applied kinesthetic feedback with constant damping on each finger. In contrast to the interaction with rigid objects using collision boundaries, fluid does not have a discernible boundary. To address this, we introduce the *sustained effect* where the system

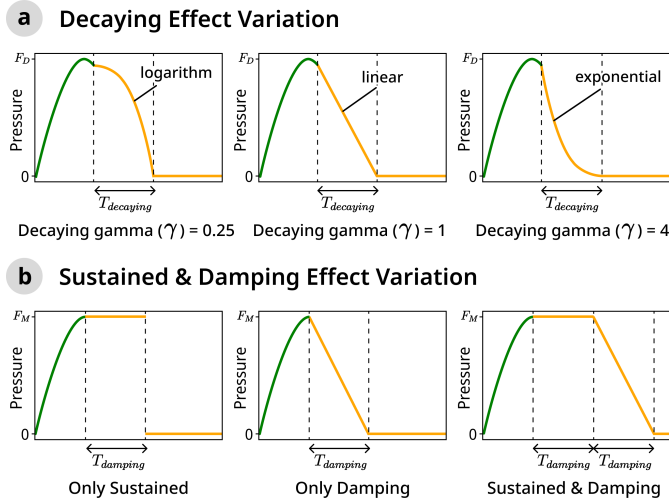


Fig. 4. Pressure variation profiles of the haptic actuator as a function of the gamma parameter. (a) Decaying profiles simulate the smoothness of fluid by inflating and deflating a pneumatic tacter. (b) Sustained and damping profiles reproduce the perceived mass of the fluid by maintaining and releasing the force through a retractuator.

briefly holds the added mass force and then applies *damping effect* with a linearly decreasing force based on the spring model. Additionally, since the just-noticeable difference (JND) of kinesthetic force perception is less sensitive than tactile feedback (around $0.5 \text{ N} \sim 1 \text{ N}$), humans struggle to discern subtle variations in gradually changing forces [48], [74].

The durations of *sustained effect* and *damping effect* are both set empirically to the *damping duration* to maximize perceptual distinction. Previous studies on force feedback have shown that longer feedback durations enhance perceived force magnitude and realism [75]. Since the added mass is a virtual force, we reasoned that users may perceive a greater force on their fingers to effectively simulate stopping or redirecting fluid flow in an accelerating underwater environment.

b) Occluded Region: If the user bends their fingers, there will be a region where the fluid is not reaching the palm. To account for this perceptually appropriate occlusion based on the bending degree, we define an *occluded region* on the palm where tactile feedback is not rendered. Since each finger bends in 1-DoF, either flexion or extension, we consider the palm area aligned with each finger to be included in the same haptic rendering region as the corresponding finger. For the thumb, however, detecting the occluded areas of the palm is complex due to the high DoFs of the carpometacarpal (CMC) joint. Thus, we exclude the thumb movement and set the occluded region to be sufficiently covered with other fingers (Fig. 7).

IV. AQUAHPATICS HAPTIC RENDERING

We performed a haptic rendering pipeline based on three main algorithms to convey drag and added mass forces in a virtual underwater. The overall pipeline in Fig. 5 shows how to operate all algorithms, including 1) drag force perception, 2) added mass force perception, and 3) occluded region detection. By using the HaptX API, we directly controlled each tacter rendering boundaries and retractuators.

A. Algorithm 1: Drag Force Perception with Movement-reflected Elements

When users move their hand with normal or lateral motions in Fig. 5, they receive drag force feedback on the palm. After updating the movement direction and F_D in each region, the *decaying effect* is applied immediately when the hand pauses. We designed this decaying variation to enhance the smoothness of the fluid sensation rendered by tactile feedback [64].

To simplify the representation of fluid pressure reduction, we employed the polynomial-based equation used for human tactile perception [76], similar to 1) logarithmic, 2) linear, and 3) exponential profiles shown in Fig. 4 (a). To figure out which profile shape better represents the fluid's smoothness property, we chose the gamma parameter (γ) as 0.25, 1, and 4 from the previous work [76]. Since *decaying effect* is attenuated based on the previously computed F_D of each boundary, pressure decaying begins at time t when the hand's velocity is lower than a specific threshold using Eq. 5.

$$F_D = \begin{cases} F_D, & (x \leq t) \\ F_D \left(1 - \frac{x-t}{T_{decaying}}\right)^\gamma, & (t < x \leq t + T_{decaying}) \end{cases} \quad (5)$$

The term $T_{decaying}$ refers to a decaying duration for maintaining the *decaying effect*. Both the rendering intensity and the decaying duration are proportional to the hand's movement speed, as faster motions require more time for the surrounding fluid to stabilize. We defined $T_{decaying}$ for both normal and lateral motions, and $T_{lateral}$ specifically for lateral motion.

a) Decaying Duration: To prevent abrupt fluctuations from the game engine and maintain the constant stance of the fluid, we used the average hand velocity (\bar{v}_h), calculated from speeds along the same directional vector.

$$T_{decaying} = \frac{\bar{v}_h}{V_h}. \quad (6)$$

V_h indicates the maximum speed of the human hand, which we set as 2.5 m/s [77]. The decaying duration was defined as $0 \leq T_{decaying} \leq 1$. To identify the most suitable duration based on $T_{decaying}$ under the *static fluid* assumption, we examined three scaling conditions $0.5\times$, $1\times$, and $2\times$ of $T_{decaying}$ for the user study.

b) Sine Wave Overlap Intensity: For lateral motion, the haptic rendering order is defined opposite to hand movement. Each lateral region generates the pre-calculated value F_D during its assigned lateral duration. We propose lateral rendering with sine waveforms using Eq. 7 on the palm [71] to produce a continuous lateral sensation [78]. To enhance the continuity of fluid flow sensation, we applied gradient overlapping between lateral boundaries during feedback rendering (see Fig. 6).

$$F_D = F_D \times \sin(2\pi t). \quad (7)$$

c) Lateral Duration: When computing $T_{lateral}$, we set the minimum (T_{min}) and maximum (T_{max}) durations maintained at each lateral boundary. To achieve a consistent fluid-flowing sensation within a single rendering cycle, $T_{lateral}$ depends on both the hand movement and speed. The faster the

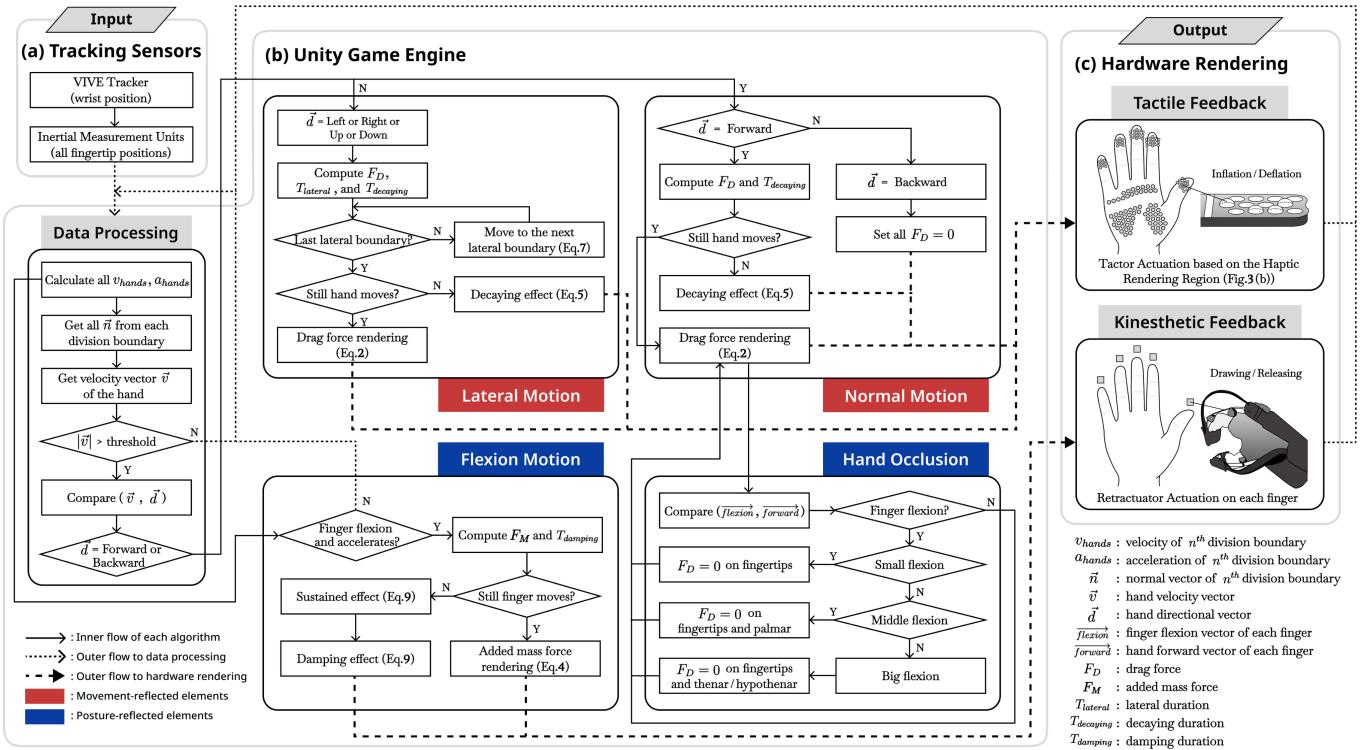


Fig. 5. Overall haptic rendering pipeline of AquaHaptics consists of corresponding equation numbers. (a) We obtain hand positions from tracking sensors. (b) Then, we compute fluid forces for each motion and (c) render multimodal haptic feedback using actuators.

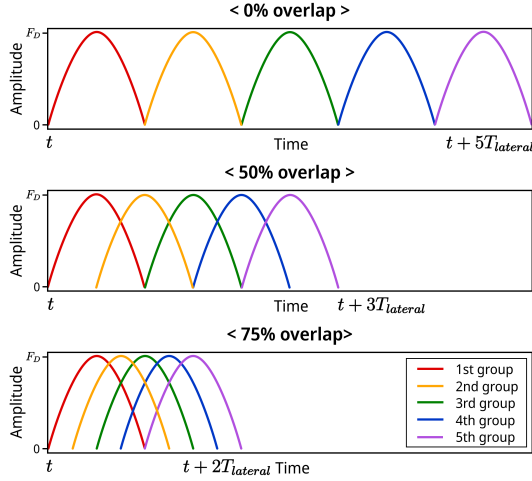


Fig. 6. Inflation and deflation of a pneumatic tactor with different overlap ratios during lateral motion. One group in each lateral region is rendered for $T_{lateral}$. A higher overlap ratio yields a shorter total rendering time.

hand speed, the shorter $T_{lateral}$ the fluid stays on the palm. Thus, $T_{lateral}$ is measured as an inversely proportional ratio based on each slow and fast speed of hand motion.

$$T_{lateral} = T_{max} - \frac{\overline{v_h}}{V_h} \times (T_{max} - T_{min}). \quad (8)$$

In our implementation, the maximum and minimum velocity of human arm movement were set to 2.5 m/s (fast) and 0.5 m/s (slow), corresponding to durations of 0.26s and 1.2s , respectively [77], [79]. Since we defined five lateral

rendering regions for all lateral motions, we divided the total duration by five for $T_{lateral}$ and allocated it to each lateral region. By allowing a tolerance 0.1s when matching the two durations with the hardware rendering, we finalized T_{max} as 0.35s and T_{min} as 0.15s , resulting in $T_{lateral}$ as $0.15\text{s} \leq T_{lateral} \leq 0.35\text{s}$.

B. Algorithm 2: Added Mass Force Perception with Posture-reflected Elements

When a finger accelerates in a virtual underwater environment, fluid inertia generates an added mass force. After calculating F_M , a *sustained/damping effect* is exerted on each finger once flexion ceases at time t . This process begins with a *sustained effect* lasting for $T_{damping}$, followed by a *damping effect* for $T_{damping}$ with linear damping using Eq. 9. For the thumb, which has a higher DoF (3-DoFs) than the other four fingers (2-DoFs), the movement of the interphalangeal (IP) joint is included.

$$F_M = \begin{cases} F_M, & (x \leq t + T_{damping}) \\ F_M \left(1 - \frac{x-(t+T_{damping})}{T_{damping}}\right), & (t + T_{damping} < x \\ \leq t + 2T_{damping}) \end{cases} \quad (9)$$

a) Sustained & Damping Duration: $T_{damping}$ is the duration for maintaining each sustained or damping effect, proportional to finger velocity. In Eq. 10, V_f denotes the maximum finger velocity, and \overline{v}_f indicates the average finger velocity. We set V_f to 1 m/s ($\approx \omega \times l_{finger}$) [80], giving a

damping duration range of ($0 \text{ s} \leq T_{damping} \leq 1 \text{ s}$). Under the *static fluid* assumption, we considered three duration scaling factors $0.5\times$, $1\times$, and $2\times$ of $T_{damping}$ to determine the most suitable parameter for the user study.

$$T_{damping} = \frac{\bar{v}_f}{V_f}. \quad (10)$$

C. Algorithm 3: Occluded Region Detection

From the perspective of the fluid flow approaching normal to the palm, occluded regions are determined by fingertip positions, indicating where the fluid no longer reaches the palm. The detection method below was derived empirically. The occlusion boundary in Fig. 7 (a) corresponds to lateral (left or right) boundaries. We defined three occlusion levels to evaluate perceptually realistic coverage by suppressing fluid pressure on the palm. In the 3-level configuration, the outermost black-rectangle region is wider than the white-pentagon region, reflecting the distance between the palmar and the upper thenar and hypothenar regions. In the 4-level configuration, the pinky could not deactivate more tactors than in the 3-level case due to its shorter length and smaller coverage area.

Fig. 7 (b) shows the method of occluded region detection. While previous work employed vector-based detection [81] or opposing forces to prevent penetration [82], our approach defines projected regions onto the palm by finger flexion rather than relying on position- or volume-based force computation. We defined a *flexion vector* extending from each MCP joint to the fingertip and established its relationship with the directional *forward vector*, which is the normal vector of the palm. Given the MCP joint's flexion range of $0 \sim 90^\circ$ [83], we set the relationship between flexion and forward vectors by the cross product.

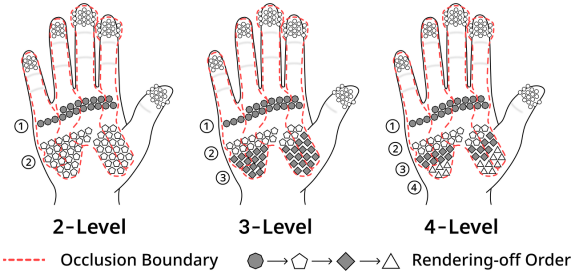
According to the result of the cross product between *forward vector* and *flexion vector*, there are three flexion cases. We designate a small flexion if the result is negative, a middle flexion if the result is near zero, and a large flexion if the result is positive, following Unity's left-handed coordinate system. Once middle flexion is reached, the palmar area becomes partially covered, and under large flexion, the hypothenar and thenar regions are sequentially occluded according to the *occlusion level*. Thus, no tactile feedback is rendered for tactors located within occluded regions.

V. USER EXPERIENCE EVALUATION

All participants wore a Varjo XR-3 (Varjo Inc.²) as a head-mounted display (HMD) and a HaptX glove on one hand during the pilot and perception studies, and on both hands during the application study. We recruited 42 unique right-handed participants, including 6 participants (2 female, mean age = 24.17, $\sigma = 3.13$) for the pilot study, 30 participants (15 female, mean age = 27.53, $\sigma = 4.09$) for the perception study, and 12 participants (6 female, mean age = 23.92, $\sigma = 3.99$) for the application study. Our study was approved by the Institutional Review Board (IRB) prior to its conduct.

²<https://varjo.com/>

a Occlusion Cases for Tactile Rendering-off



b Detection of the Occluded Region

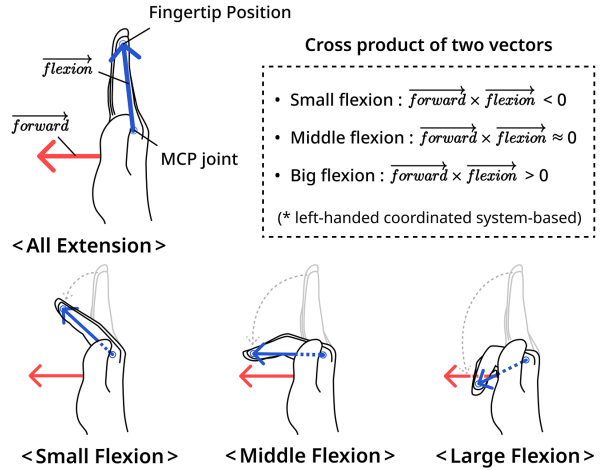


Fig. 7. (a) Occlusion levels and boundaries on the palm deactivate tactile feedback during finger flexion. (b) Occluded regions on the palm are determined by the relationship between the flexion vector and the forward vector.

A. Study Setup

For all studies, we installed two HTC Vive base stations in front of participants to track wrist positions. We used the Unity engine to conduct the studies in a VR environment with real-time control of HaptX gloves. To reduce the noise from the pneumatic air compressor, participants wore a noise-canceling headset, as shown in Fig. 8.

B. Pilot Study: Overlap Ratio for Lateral Haptic Rendering

As mentioned earlier, the total duration of lateral rendering decreases as the overlap ratio increases. In this study, we aimed to examine the perceived fluid continuity and realism of the rendered flow and to determine whether different overlap ratios lead to perceptual discrepancies. We set the speed of lateral haptic rendering on the palm to 0.5 m/s [77] to ensure users could distinguish lateral continuity at lower speeds.

Since higher overlap ratios enhance lateral sensation have been confirmed, we focused on previously explored medium [45] and large ratios [44] with a 0% baseline. All participants fixed their right palms upward and then just felt the constant fluid flowing over them. We collected responses from a total of 216 trials consisting of 4 directions (left, right, up, and down) \times 3 ratios (0%, 50%, and 75%) \times 3 sessions \times 6 participants. We asked participants to imagine that the fluid flows in the opposite direction from the lateral sweeping direction. All trials were carried out in a randomized order.

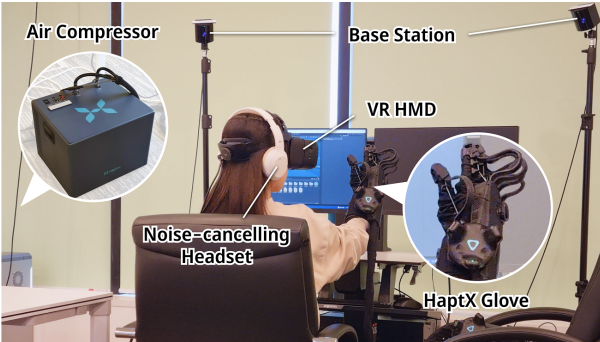


Fig. 8. Experimental setup for the user study in VR with haptic gloves. The participant wears a haptic glove, and the air compressor is placed on the floor.

After each trial, participants verbally rated the perceived continuity and realism of the flowing water on a 7-point Likert scale, following a format similar to that used in prior work [45]. We asked “*Q1. How continuous was the lateral water flow being rendered?*”, and “*Q2. How consistent was the sensation of water flow on the palm with the real world?*”. Fig. 9 shows the responses from the participants. Consistent with previous findings [45], higher overlap ratios presents higher scores for both continuity and realism, even when using pneumatic-based haptic rendering on the hand. After each session, we got qualitative answers describing the fluid sensation they experienced during the study.

From the result of two-way repeated measures (RM) ANOVA, *overlap ratio* had a significant effect on both continuity ($F(2, 10) = 11.55, p = .02$ with $\eta^2 = .25$) and realism ($F(2, 10) = 9.97, p = .02$ with $\eta^2 = .41$), while *direction* had a meaningful impact only on realism ($F(3, 15) = 5.57, p = .03$ with $\eta^2 = .05$).

All participants generally mentioned that “*The higher the overlap ratio, the stronger and more continuous the perceived fluid flow. The no-overlap condition felt discontinuous and unnatural.*” They also noted that “*All lateral directions were clearly distinguishable by the differentiated lateral fluid rendering.*”. Additionally, P4 said that “*When the fluid rendering occurred to the left direction on the palm, the duration staying on the thumb was relatively short compared to fluid rendering to the right. So it felt like skipping around the thumb area.*”. P6 responded that “*In the case of up and down motion, I felt relatively less fluid-flowing sensation than left and right motion. Because the fluid feedback from the fingertip to the palmar was instantly transferred.*”.

In this regard, we adjusted the lateral rendering duration by reflecting each length of the hand part according to hand anatomy [62]. Fig. 10 illustrates the final haptic rendering duration based on the initial lateral duration $T_{lateral}$. Since we confirmed that *overlap ratio* is a critical factor in the continuous and realistic fluid sensations, we selected the ratio of 0.75 for the final lateral rendering configuration.

C. Perception Study: Finding Fluid Property Parameters for Proposed Algorithms

To provide haptic rendering through pneumatic actuators, it is necessary to designate proper duration and pressure values

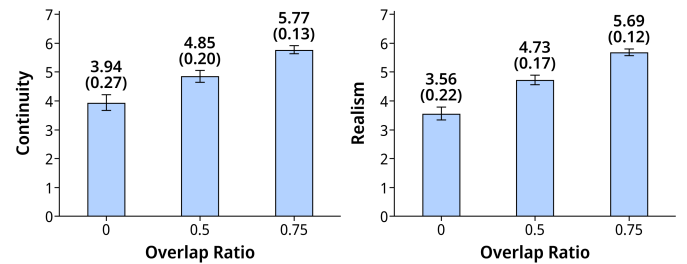


Fig. 9. Average scores for continuity and realism of fluid flow for different overlap ratios. Error bars and parenthesized numbers indicate standard error.

that evoke realistic fluid sensations while satisfying human perception. For comparison with real-world water experiences as in [26], we set up a water tank ($0.35\text{m} \times 0.22\text{m} \times 0.28\text{m}$) filled with water at about 18°C . Before proceeding with a VR study, we asked all participants to dip one hand into the water tank and perform repetitive motions, focusing only on the water pressure sensation above the palm.

In the VR scene, participants moved their hand between the two spheres for each forward or lateral direction (Fig. 11). When a red light appeared on the target sphere, they followed a moving cube that guided the hand motion. During the flexion motion, participants synchronized their finger bending with the cube’s flexion and extension movement. The reason for placing that cube guidance was to reduce the speed of the hand or finger movement deviation among participants.

The pressure profiles applied during each motion in the perception study are presented in Appendix A. Statistical analysis of the user study was conducted using repeated-measures (RM) ANOVA to evaluate mean differences across dependent variables, following the prior work [76].

1) Drag Force Perception: To feel the fluid sensation on the palm, participants moved their right hand repeatedly in forward and backward directions for the forward motion-induced feedback, and left and right directions for the lateral motion-caused feedback.

During each forward and lateral motion, we collected 2,700 trials consisting of (non-decaying + 3 durations ($0.5\times, 1\times, 2\times$) \times 3 decaying gammas ($0.25, 1, 4$)) \times 3-repetitive paired movements (forward-back or left-right) \times 3 sessions \times 30 participants. The first session served as training, and we only analyzed the data from last two sessions. A balanced Latin square design was used to counterbalance the trial order. After each trial, participants rated their perceptions using a 100-point scale in response to the following questions; “*Q1. (Smoothness) The interval of fluid pressure decreasing on the palm was smooth.*”, “*Q2. (Continuity) The duration of fluid pressure decreasing on the palm was continuous.*”, and “*Q3. (Realism) The sensation of fluid pressure decreasing on the palm was consistent with the real world.*”.

We regarded a non-decaying case (no $T_{decaying}$ and no γ) as a baseline and conducted one-way RM ANOVA in a total of 10 decaying cases. We then compared the baseline with the other 9 decaying cases by the post-hoc paired t-test. Next, we applied a two-way RM ANOVA among 9 decaying cases, except a baseline, to confirm the interaction effect between

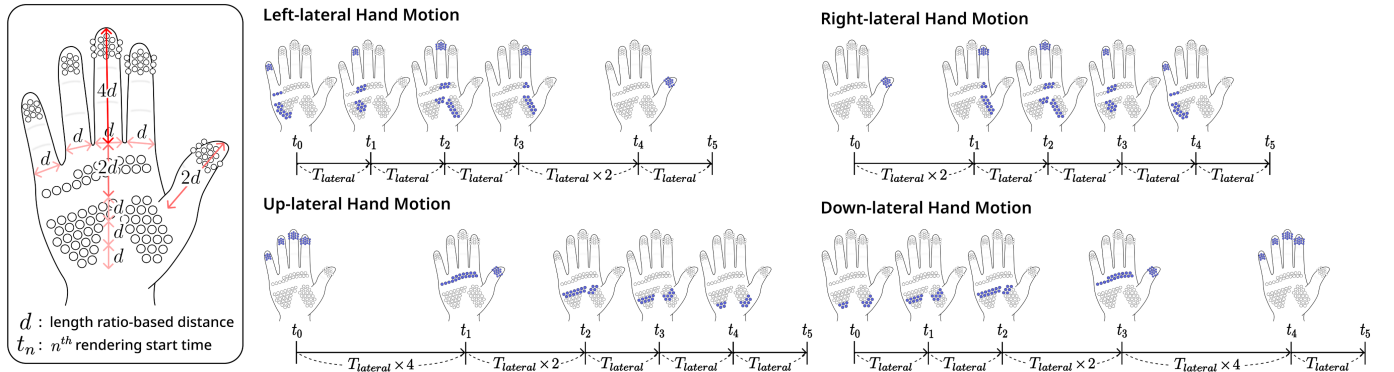


Fig. 10. Lateral haptic rendering on the palm. Rendering duration for each lateral motion is set according to pilot study results, with the left-hand sequence reversed relative to the right hand.

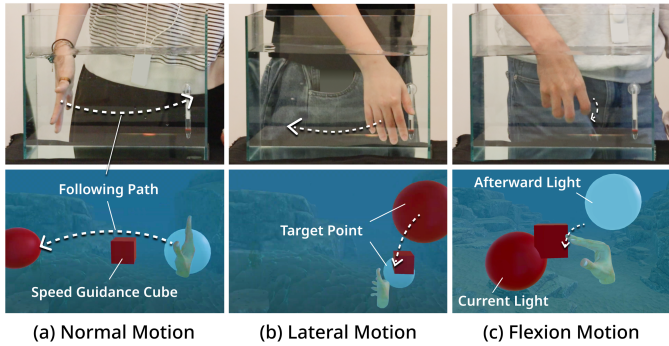


Fig. 11. Cube-guided motion task. The cube moves between two spheres, with a red light indicating the target sphere. Participants followed the cube using either (a), (b) hand, or (c) finger. (Top: real-world experience setup; Bottom: VR scene.)

two independent variables, *Duration* and *Gamma*. All pairwise comparisons were based on Bonferroni corrections. Fig. 12 shows the average scores from the study.

a) *Smoothness*: The results of the one-way RM ANOVA revealed a significant difference among all decaying cases for both forward ($F(9, 261) = 16.279, p < .001$ with $\eta^2 = .121$) and lateral motions ($F(9, 261) = 14.158, p < .001$ with $\eta^2 = .106$). Paired t-tests indicated significant differences in all decaying cases compared to the baseline, except when $\gamma = 0.25$ with all 3 durations ($0.5\times, 1\times, 2\times$) for both motions. Only one case ($1\times, \gamma = 1$) in the lateral motion showed a marginal effect ($p = .022$), while all other cases indicated $p < .01$. These findings suggest that decaying cases generally differ from the baseline in perceived smoothness for both motions, except when $\gamma = 0.25$.

The two-way RM ANOVA showed that both *Duration* ($F(2, 58) = 5.184, p = .011$ with $\eta^2 = .008$) and *Gamma* ($F(2, 58) = 24.158, p < .001$ with $\eta^2 = .089$) significantly affected smoothness in the forward motion, while only *Gamma* ($F(2, 58) = 28.233, p < .001$ with $\eta^2 = .094$) had an effect in the lateral motion. There was no interaction effect between the two variables for both motions. In the post-hoc analysis, pairwise comparisons revealed significant differences across all *Gamma* levels, with the strongest effect between $\gamma = 0.25$ and $\gamma = 4$ for both forward ($p < .001, g =$

-0.764) and lateral motions ($p < .001, g = -0.718$). These results suggest that higher *Gamma* values directly enhance the perceived smoothness of fluid sensation.

b) *Continuity*: The one-way RM ANOVA revealed significant differences among all decaying cases for both forward ($F(9, 261) = 12.691, p < .001$ with $\eta^2 = .101$) and lateral motions ($F(9, 261) = 13.549, p < .001$ with $\eta^2 = .099$). However, the paired t-test indicated no significant difference from the baseline in forward motion when *Duration* was $0.5\times$ for any *Gamma* ($0.25, 1, 4$) or when *Duration* was $1\times$ with $\gamma = 1$. For lateral motion, only when *Duration* was $0.5\times$ with $\gamma = 0.25$ had no significant difference. All other cases exhibited meaningful differences ($p < .01$) for both motions. This suggests that short *Duration* (such as $0.5\times$) does not produce a notable difference compared to the baseline.

From the results of the two-way RM ANOVA, only *Duration* had a significant effect on both forward ($F(2, 58) = 23.544, p < .001$ with $\eta^2 = .064$) and lateral motions ($F(2, 58) = 22.367, p < .001$ with $\eta^2 = .065$). There was no interaction effect between *Duration* and *Gamma*. In the post-hoc analysis, pairwise comparisons showed the *Duration* demonstrates a meaningful influence on continuity, especially between $0.5\times$ and $2\times$ for both forward ($p < .001, g = -0.658$) and lateral motions ($p < .001, g = -0.662$). These results highlight that longer *Duration* enhance the perceived continuity of the fluid.

c) *Realism*: Realism is the most important factor in selecting parameter values suitable for human perception. The one-way RM ANOVA showed significant differences among all decaying cases for both forward ($F(9, 261) = 10.828, p < .001$ with $\eta^2 = .095$) and lateral motions ($F(9, 261) = 11.307, p < .001$ with $\eta^2 = .109$). From the paired t-test in forward motion, significant differences appeared in all cases except when $\gamma = 0.25$ with every 3 durations ($0.5\times, 1\times, 2\times$) compared to the baseline. In lateral motion, two cases ($0.5\times$ with $\gamma = 4, 2\times$ with $\gamma = 4$) had moderate effects ($p < .05$), and two other cases ($0.5\times$ with $\gamma = 1, 1\times$ with $\gamma = 4$) showed notable differences ($p < .01$) from the baseline.

In the result of two-way RM ANOVA, only *Gamma* significantly contributed to realism, and there was no impact of *Duration* for both motions. Each influence of *Gamma* showed $F(2, 58) = 15.472, p < .001$ with $\eta^2 = .061$ in

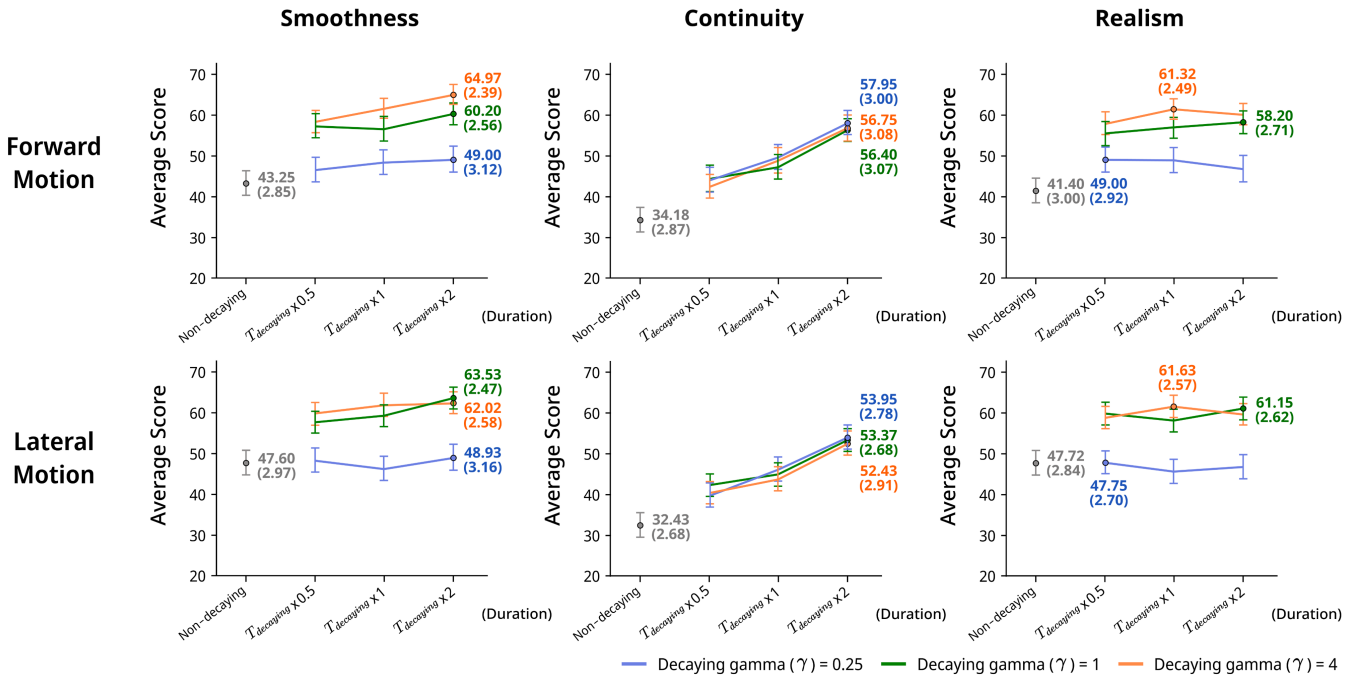


Fig. 12. The highest scores for smoothness, continuity, and realism as functions of γ and $T_{decaying}$ during forward or lateral motion. Error bars represent the standard error.

forward, and $F(2, 58) = 25.623, p < .001$ with $\eta^2 = .104$ in lateral motion. There was no interaction effect between the two variables. Post-hoc analysis revealed significant differences of *Gamma* between 0.25 and 4 particularly for both forward ($p < .001, g = -0.630$), and lateral motions ($p < .001, g = -0.755$). These results indicate that the high value of *Gamma* provides more realistic fluid sensations.

During the in-depth interview, we compared the qualitative responses received by participants to the statistical results. With regard to the normal motion with the drag force, most participants felt that the decaying pressure was smoother when the pressure decreased quickly (an exponential decaying) and preferred that case with $\gamma = 4$. Some participants stated, “*It was quite similar to the real sense of water when I gave the high score in realism.*” (P5, P8, P15, P19, P21). However, perceptions of realism varied with *Duration*.

For lateral motion with drag force, most participants felt that faster decaying pressure enhanced both realism and smoothness. Some noted, “*Since resistance on the sides of the hand was strongest in real water, the feeling of water on the palm was less. Although it differs from the real that water does not sweep on the entire palm, it still provides a convincing sense of continuous fluid, especially in a virtual underwater scene.*” (P2, P4~7, P9~10, P12, P14~15, P21~22, P26). Overall, most participants preferred stronger tactile sensations in VR compared to the light sense in real water.

Therefore, we suggest that it is cognitively better applying *decaying effect* where the pressure decreases smoothly, even if the human hand stops feeling the smoothness and continuity of the fluid, than strictly following a physics-based formula. We adopted the medium length (**Duration** = $1 \times T_{decaying}$) and fast reduction (**Gamma** = 4) for both forward and lateral

motions to maximize perceived realism and smoothness.

2) *Added Mass Force Perception*: To feel the sensation of fluid mass through the fingers, participants repeatedly performed flexion and extension movements. For the finger flexion study, we conducted the overall 4500 trials containing (Non-sustained and damping + 3 conditions (only sustained, only damping, sustained & damping) \times 3 durations ($0.5 \times, 1 \times, 2 \times$) \times 5-repetitive paired movements (flexion/extension) \times 3 sessions \times 30 participants. The trial order was counterbalanced using a Latin square design, and only responses from the last two sessions were analyzed. After each trial, participants rated their perception using a 100-point scale to the following questions; “Q1. (*Heaviness*) The added mass of water pressure felt on the fingers was heavy.”, “Q2. (*Continuity*) The duration of water pressure decreasing on the finger was continuous.”, and “Q3. (*Realism*) The added mass sensation induced by the inertia of surrounding water was consistent with the real world.”. The measure of heaviness, which differs from the previous study, represents the perceived degree of mass or resistance when moving a finger through accumulated water.

We considered a non-sustained and damping case (no duration for both sustained and damping effect) as a baseline and conducted one-way RM ANOVA across all 10 sustained and damping cases. We then compared the baseline with the other 9 sustained and damping cases in the post-hoc test. A two-way RM ANOVA among 9 sustained and damping cases without a baseline was also performed to examine the interaction effect between two variables, *Condition* and *Duration*.

a) *Heaviness*: During the finger flexion motion, all sustained and damping cases had an impact compared to the baseline in heaviness (Fig. 13). Especially, *Condition* with only sustained has the highest score in general compared

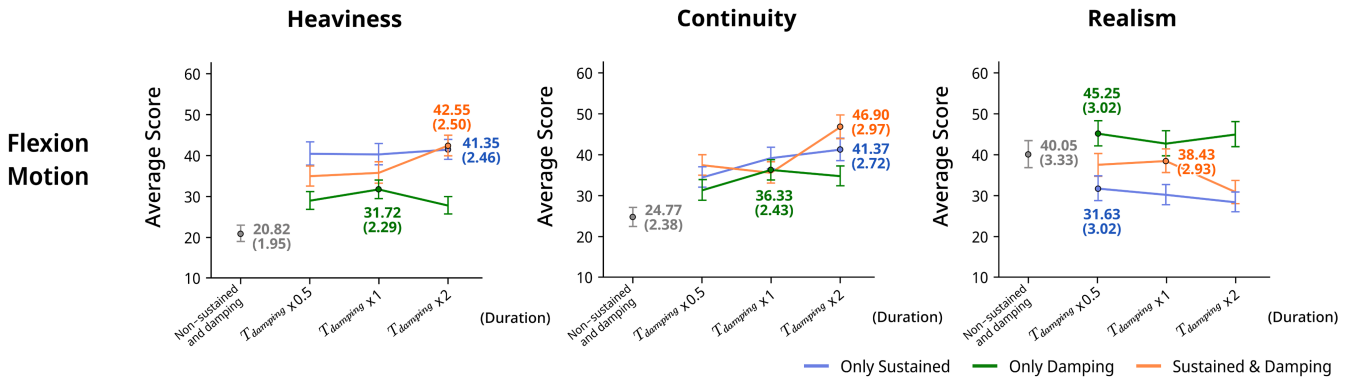


Fig. 13. Highest scores for heaviness, continuity, and realism as functions of condition and $T_{damping}$ during finger flexion. Error bars represent the standard error.

to the other two conditions. The result of one-way RM ANOVA showed a significant difference across all sustained and damping cases ($F(9, 261) = 15.584, p < .001$ with $\eta^2 = .139$). In the paired t-test analysis, only one case ($2\times$ with only damping) indicated no meaningful difference from the baseline. Two cases ($0.5\times$ with only damping, $1\times$ with only damping) showed moderate differences $p < .05$ and the others showed highly significant effects $p < .001$.

The two-way RM ANOVA further revealed only *Condition* ($F(2, 58) = 22.213, p < .001$ with $\eta^2 = .071$) effects significantly on heaviness. And there was an interaction effect between *Condition* and *Duration* ($F(4, 116) = 2.968, p = .049$). Post-hoc analyses revealed a strong effect on *Condition*, indicating the only damping condition differed significantly from both only sustained ($p < .001, g = -0.702$) and sustained & damping ($p < .001, g = -0.54$). For the interaction between *Condition* and *Duration*, meaningful differences were observed specifically with the $2\times$ duration between only damping and only sustained ($p < .001, g = -0.832$), and between only damping and sustained & damping with $2\times$ ($p < .001, g = -0.880$). This indicates that *Condition* with only sustained or sustained & damping substantially increases the perceived heaviness than only damping.

b) *Continuity*: The one-way RM ANOVA revealed a significant difference among all sustained and damping cases ($F(9, 261) = 10.293, p < .001$ with $\eta^2 = .091$). However, the paired t-test showed no notable differences from the baseline when *Condition* was only sustained with $0.5\times$, or only damping with $0.5\times$, and $2\times$. The other cases had $p < .01$, except the only damping with $1\times$ ($p = .02$).

In the two-way RM ANOVA, both variables *Condition* ($F(2, 58) = 5.15, p = .01$ with $\eta^2 = .019$) and *Duration* ($F(2, 58) = 14.86, p < .001$ with $\eta^2 = .022$) denoted a significant impact on continuity. The interaction effect between them had appeared ($F(4, 116) = 4.41, p = .01$). Pairwise comparison indicated that the long duration ($2\times$) produces a more continuous feeling of the fluid mass. The sustained & damping showed a significant influence compared to the only damping in *Condition* ($p = .024, g = 0.349$) and in the interaction effect with the long duration $2\times$ ($p = .003, g = 0.64$). It means that *Condition* sustained & damping with longer *Duration* enhances the perceived continuity of the fluid mass.

c) *Realism*: For realism, the highest mean scores were observed when the *Condition* was only damping. Although the one-way RM ANOVA showed significant differences among all sustained and damping cases ($F(9, 261) = 11.670, p < .001$ with $\eta^2 = .076$), no pairwise t-test revealed a significant difference from the baseline.

The two-way RM ANOVA showed significant main effects for both *Condition* ($F(2, 58) = 41.280, p < .001$ with $\eta^2 = .005$) and *Duration* ($F(2, 58) = 3.565, p = .036$ with $\eta^2 = .075$) with no interaction effect. Post-hoc comparisons revealed significant differences in *Condition* between only damping and only sustained ($p < .001, g = 0.7$), indicating a large effect size. For the interaction between *Condition* and *Duration*, significant influences were observed between only damping and only sustained ($p < .001$), regardless of *Duration*. This indicates that *Condition* with only damping most effectively enhances the perceived realism of fluid mass.

In the in-depth interview, most participants said that strong mass or resistance during finger flexion felt awkward. They noted, “*The feeling of the continuous gradual reduction of the force was the best.*” when the damping effect was provided. Conversely, several participants commented, “*It was perceived as the least realistic when the applied force abruptly terminated midway in some trials.*” (P1, P4~6, P8, P10, P13, P20~21, P23, P28, P30) when the sustained effect was rendered. Some participants specifically described the sensation, “*When it’s heavy about the breaking force, it felt like snow clumping together, or something feels like stirring up a massive mud.*” (P15, P17). There were answers about further improvements, “*I felt more resistance when I extended my fingers than bending them in real water, so it would be better if there was also greater resistance on the dorsal side.*” (P2, P11, P14, P17, P21~22).

Based on the statistical results and qualitative answers, we conclude that delivering only a *damping effect* with a short duration best conveys the sensation of the light fluid mass. Therefore, we chose the continuous attenuation (**Condition** = *only damping*) and short duration (**Duration** = $T_{damping} \times 0.5$) for realistic fluid mass.

3) *Discrimination of Occluded Region*: To achieve a reasonable occluded resolution on the palm, we used different rendering-off levels (see Fig. 7). Tactile pressure was con-

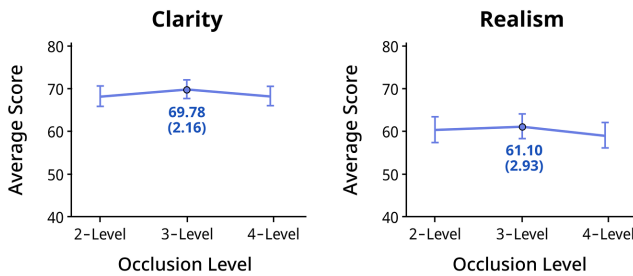


Fig. 14. Highest scores for occlusion clarity and realism as a function of occlusion level during finger flexion. Error bars represent the standard error.

tinuously provided on the palm while participants bent their fingers slowly following cube guidance as in the previous study, feeling the sense of fluid that did not reach the palm.

We conducted the overall 1,350 trials including 3 resolutions (2-level, 3-level, 4-level) \times 5-repetitive paired movements (flexion-extension) \times 3 sessions \times 30 participants. The order of all trials was used by a complete counter-balanced Latin square. After each trial, participants rated two questions on a 100-point scale; “Q1. (Occlusion clarity) The water pressure did not contact the palm was clear depending on the degree of finger bends.” and “Q2. (Realism) The water pressure did not contact the palm by bending my fingers was consistent with the real world.”.

The one-way RM ANOVA revealed no significant effect of *Resolution* on either clarity ($F(2, 58) = 0.662, p = .520$ with $\eta^2 = .002$) or realism ($F(2, 58) = 0.598, p = .553$ with $\eta^2 = .001$).

Compared to the previous study, most participants said they felt the least difference during this experience. They additionally answered, however, “The realism score set high was based on the most naturally occluded parts according to the speed of my finger bending.” (P3~10, P14~15, P19~20, P22, P25, P30). Participants also noted that occlusion was easier to recognize during finger extension than flexion. Although differences were minor, we chose the middle level (**Resolution** = 3-level), which showed the highest average realism score, as the occlusion resolution on the palm during finger bending.

D. Application Study: Underwater Swimming Experience

We derived fixed parameters from the perception study and conducted the application study. To analyze the overall haptic sensation with our established rendering algorithm, participants wore both gloves and implemented a given underwater scenario (see Fig. 15). They were instructed to move forward by swimming with both hands (without actual body movement) and to reach a target location within a time limit while maintaining a comfortable hand posture.

The system enables real-time visuo-haptic interaction between a Unity-based VR environment and a pneumatic glove interface. The Unity framework operated above 54 FPS, where visual rendering was dominated by VR setup and camera processing. The haptic rendering loop ran at 1 kHz, while the glove system exhibited a maximum latency of 20 ms for motion capture and 30–35 ms for pneumatic actuation. Overall,

TABLE I
HAPTIC RENDERING CONDITIONS DURING THE APPLICATION STUDY

	Directional vector	Rendering region	Overlap ratio	Decaying effect	Damping effect	Occluded region
Baseline	O	X	X	X	X	X
Movement	O	O	O	O	X	X
Baseline & Posture	O	X	X	X	O	O
Movement & Posture	O	O	O	O	O	O

the integrated pipeline maintained an overall system latency of approximately 16–20 ms, ensuring stable and continuous visuo-haptic feedback.

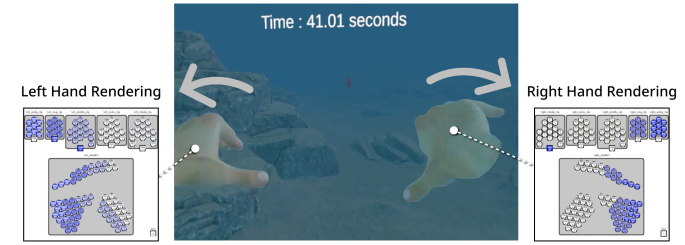


Fig. 15. Underwater swimming scenario used in the application study.

Based on Eq. 1, we investigated how the individual elements of hand movement and posture contribute to immersion and overall user experience under four experimental conditions. In the Table. I, it lists the movement-reflected and posture-reflected elements described in Section 3.2.

The *Baseline* provides simple tactile feedback with only a directional vector and uniform pressure across the hand, without spatial rendering. *Movement* delivers full tactile feedback, and *Baseline & Posture* adds kinesthetic feedback on uniform tactile feedback. *Movement & Posture* provides full tactile and kinesthetic feedback, reflecting the maximum rendering capability of the haptic gloves. Pressure profiles for all conditions during the application study are provided in Appendix B.

We conducted the qualitative study using a balanced Latin square. After each trial, participants rated measures on a 7-point Likert scale, adapted from prior works [84], [85]. Fig. 16 illustrates the average scores across all measures.

- (*Realism*) How consistent was the sensation of fluid pressure on your hands with the real world?
- (*Naturalness*) How natural was the haptic feedback provided according to the hand's movement and posture?
- (*Involvement*) How involved were you in the virtual underwater through the haptic feedback as part of the experience?
- (*Effectiveness*) How effective do you feel the haptic feedback is in feeling the fluid sensation?
- (*Satisfaction*) How much do you like integrating the haptic feedback to experience the virtual underwater?

A one-way ANOVA with Tukey's HSD post-hoc test revealed significant effects of rendering condition for all measurements. It showed (*Realism*; $F(3, 44) = 3.252, p = .031$), (*Naturalness*; $F(3, 44) = 3.786, p = .017$), (*Involvement*; $F(3, 44) = 5.544, p = .003$), (*Effectiveness*; $F(3, 44) = 4.857, p = .005$), and (*Satisfaction*; $F(3, 44) = 7.392, p < .001$). Post-hoc comparisons showed significant differences

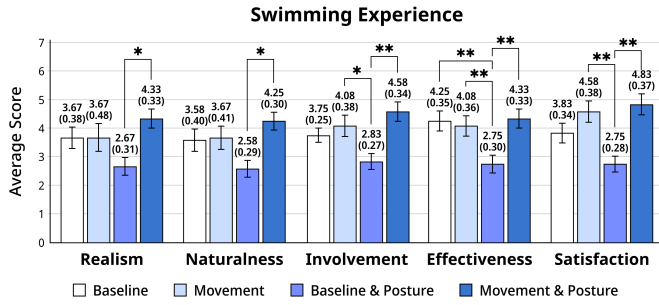


Fig. 16. Scores for realism, naturalness, involvement, effectiveness, and satisfaction are reported for different rendering conditions during underwater haptic feedback. Error bars and parenthesized numbers indicate standard error.

between *Baseline & Posture* and *Movement & Posture* for *Realism* ($p = .017$) and *Naturalness* ($p = .010$). For *Involvement* and *Satisfaction*, *Baseline & Posture* differed significantly from both *Movement* ($p = .035$ and $p = .003$) and *Movement & Posture* ($p = .002$ and $p = .001$), respectively. For *Effectiveness*, *Baseline & Posture* differed significantly from all other conditions; *Movement* ($p = .037$), *Baseline* ($p = .015$), and *Movement & Posture* ($p = .010$).

Most participants preferred the sensation of the sequential fluid flowing across the palm when they moved forward while shaking both hands. This includes *Movement* condition reflecting the lateral rendering, which participants described this as a rich and dynamic tactile experience. In contrast, since the *Baseline & Posture* condition includes occlusion elements, reduced the perceived fluid sensation with tactile feedback when bending fingers. A key point to note here is that the *Movement & Posture* condition received common feedback “*It feels more perceptible fluid resistance, which leads to a realistic and natural sensation delivered to the hand.*” (P3~12). From this study, we found that hand-specific feedback and unexplored multimodal characteristics provide users with a more realistic and immersive underwater experience.

VI. DISCUSSION

With AquaHaptics, we propose fluid-haptic feedback in VR underwater with multimodal feedback. We further interpret the qualitative results from the user studies and derive design guidelines for prospective fluid-haptic rendering. Moreover, we discuss the limitations of our current implementation and the potential future work to overcome these limitations.

A. Fluid-Haptic Rendering Design Guidelines

To achieve realistic fluid sensations and align with human perception, we suggest design strategies for hand-specific elements based on fluid characteristics and haptic actuators.

a) Tactile Feedback: When simulating fluid flow across the palm during lateral hand motion, we recommend that the duration of staying per boundary ($T_{lateral}$) be proportionally adapted to the relative length of hand regions. To generate the smoothness of the fluid with perceived drag forces for both forward and lateral motion, decaying gamma (γ) has a significant impact. Since decaying pressure with logarithm ($\gamma = 0.25$)

is not much different from the baseline (non-decaying), the value of γ needs to be more than 0.25 (refer to Eq. 11), and further modulates depending on the target fluid’s smoothness. For turbulent case, such as our virtual underwater environment with high softness, values of $\gamma \geq 4$ may be required.

$$F_D \left(1 - \frac{x-t}{T_{decaying}} \right)^\gamma > F_D \left(1 - \frac{x-t}{T_{decaying}} \right)^{0.25}. \quad (11)$$

Regarding the rendering-off with the occlusion on the palm during finger bending, statistical results revealed no significant differences among different resolution levels. However, qualitative feedback indicated that too low a resolution (*2-level*) caused users to perceive the occlusion rendering as faster than their finger motion, while too high a resolution (*4-level*) led to unnatural sensations due to overly sensitive haptic responses to small movements. Although a medium resolution was suitable in our study, the optimal occluded resolution can vary according to the haptic interface used. Therefore, we suggest finding a proper resolution depending on the specific hardware characteristics while ensuring it remains within the human tactile discrimination threshold on the palm.

b) Kinesthetic Feedback: A heavy added mass of the fluid can feel unnatural during finger bending. Rather than applying *Only sustained* or *Sustained & Damping* conditions, *Only damping* generates the lightest mass sensation, which closely resembles the baseline. We therefore recommend using the *Only damping* condition with a short duration ($0.5T_{damping}$) following the finger pause (see Eq. 12). To render fluids with higher viscosity, there are three options to convey a stronger sense of mass. We can apply the *Sustained & Damping* condition maintaining the kinesthetic force for a longer duration ($n \times T_{damping}$, $n > 0.5$), or simply deliver the high rendering force. It depends on the specific physical property to be represented and can be tuned through a suitable combination. In contrast, the *Only sustained* condition is effective for rendering lumpy or granular materials, such as snow chunks or small solid particles suspended in fluid.

$$F_M = \begin{cases} F_M, & (x \leq t) \\ F_M \left(1 - \frac{x-t}{T_{damping}} \right). & (t < x \leq t + T_{damping}) \end{cases} \quad (12)$$

c) Rendering Elements: After determining the parameters based on fluid properties, we suggest combining rendering conditions to achieve a rich fluid sensation. In a VR underwater environment, movement-reflected (F_D) elements enhanced fluid sensation by conveying the fluid current over the palm. However, when posture-reflected (F_M) elements were added to the baseline, the overall user ratings were lower compared to the baseline alone. The most favorable condition was combining all movement and posture conditions ($F_D + F_M$) for an immersive and natural experience.

Unlike parameters such as decaying or damping durations ($T_{decaying}$ or $T_{damping}$) examined individually in the perception study, the application study involved conditions combining multiple hand-specific elements rather than isolated ones. In the swimming scenario, where continuous arm motion

is dominant, movement-reflected elements had a stronger perceptual influence than posture-reflected ones. This indicates that, rather than focusing on fine-grained timing, future underwater interaction designs should emphasize the coordination between hand motion and finger articulation, with feedback intensity appropriately reflects dynamic movements.

B. Limitations and Future Works

Accurately reproducing the full range of fluid effects could further enhance perceived realism. However, perception also depends on numerous factors such as fluid environment, actuator type, and the locations on the hand where forces are applied. Future studies are needed to examine these influences.

a) *Fluid Environment*: Our underwater environment assumes a static fluid, focusing primarily on drag and added mass forces while omitting secondary effects such as vortex shedding. In reality, flow separation around the hand surface can produce wake regions and vortices accompanied by perceptible vibrations. Incorporating such fluid phenomena, along with a more comprehensive temporal model of hand motion, including angular velocity, jerk, and moment of inertia, could improve the realism of the haptic experience [24].

b) *Hand Anatomy*: We defined simplified rendering regions based on anatomical divisions for lateral motion. Finer subdivision of the hand could further enhance fluid interaction. Currently, we limited the finger flexion to 1-DoF rotation and excluded the thumb motion from occlusion rendering. Incorporating higher DoFs and full-finger activation, including the thumb, is expected to yield more realistic feedback. Moreover, because subtle differences in palm occlusion were not clearly observed in our study, future work should investigate the interaction between finger flexion and palm occlusion to improve rendering fidelity.

c) *Hardware Configuration & Scalability*: The absence of factors between the palm and fingertips reduces continuity in perceived fluid flow. Adding actuators on the lateral and dorsal sides of the hand can provide richer feedback. In low-resolution setups, future work should refine tactile placement based on pressure discrimination and hand-related factors such as feedback duration and sensitivity. The intensity of kinesthetic feedback in this work was scaled within device limits in relation to the actual fluid forces. Future psychophysical studies could help determine perceptual thresholds for gradual and refined variations in force.

Our system can also support different actuator types if force adjustments are matched. For instance, rigid actuators (e.g., voice coils or solenoids) can generate decaying effects by adjusting intensity, while soft actuators [86], [87] can achieve similar effects via pressure variation. Incorporating actuators capable of wetness and thermal feedback would further enhance the sense of physical presence [88]–[90]. If the actuators extend to other body parts, utilizing drag force for lower limbs [25] or inertial force for the head [91], could broaden immersive fluid-haptic applications.

d) *Rendering Diverse Properties*: User responses indicated that we can render diverse properties with tactile and kinesthetic feedback through our hand movement- and posture-specific approaches. By adjusting parameters such as decaying

gamma, sustained condition, or damping duration through pressure variations, sensations ranging from smooth fluid to viscous mud or lumpy granular masses can be evoked. We believe that further tuning of these parameters can render additional physical properties such as viscosity, elasticity, and inertia, for a more realistic and versatile haptic experience.

VII. CONCLUSION

AquaHaptics is a multimodal haptic rendering pipeline that provides fluid feedback for immersive virtual underwater experiences. By defining the hand movement- and posture-reflected elements, we rendered drag and added mass force perceptions with pressure variations. User studies confirmed that modulating these variations produces a more realistic fluid sensation than using purely physics-based equations. Participants reported 61% similarity for smooth pressure decaying on the palm and 45% for light mass damping through the fingers compared to real water. Using perceptually tuned fluid parameters, we further conducted an underwater swimming scenario, demonstrating richer results than a baseline without detailed hand parts or diverse movements. By delivering perceivable fluid forces with multimodal feedback, AquaHaptics shows the potential to satisfy both high-fidelity rendering and human perception in immersive VR underwater. We believe our pipeline can be effectively applied in VR games, education, training, and other fluid-related applications.

REFERENCES

- [1] C. Heater, "Being there: The subjective experience of presence." *Presence Teleoperators Virtual Environ.*, vol. 1, no. 2, pp. 262–271, 1992.
- [2] M. Slater and S. Wilbur, "A framework for immersive virtual environments (five): Speculations on the role of presence in virtual environments," *Presence: Teleoperators & Virtual Environments*, vol. 6, no. 6, pp. 603–616, 1997.
- [3] M. J. Schuemie, P. Van Der Straaten, M. Krijn, and C. A. Van Der Mast, "Research on presence in virtual reality: A survey," *Cyberpsychology & behavior*, vol. 4, no. 2, pp. 183–201, 2001.
- [4] T. B. Sheridan *et al.*, "Musings on telepresence and virtual presence." *Presence Teleoperators Virtual Environ.*, vol. 1, no. 1, pp. 120–125, 1992.
- [5] R. Held and N. Durlach, "Telepresence. presence: Teleoperators and virtual environments, 1 (1), 109-112. hendrix, c, & barfield, w.(1996). presence within virtual environments as a function of visual display parameters," *Presence: Teleoperators and Virtual Environments*, vol. 5, no. 2, pp. 5–39, 1992.
- [6] L. B. Rosenberg, "Virtual fixtures: Perceptual tools for telerobotic manipulation," in *Proceedings of IEEE virtual reality annual international symposium*. Ieee, 1993, pp. 76–82.
- [7] C. Clashing, I. Smith, M. F. Montoya, R. Patibanda, S. Ananthanarayan, S. J. Pell, and F. F. Mueller, "Going into depth: Learning from a survey of interactive designs for aquatic recreation," in *Proceedings of the 2022 ACM Designing Interactive Systems Conference*, 2022, pp. 1119–1132.
- [8] M. F. Montoya, "Towards the design of playful water experiences using interactive technology," in *Companion Proceedings of the 2024 Annual Symposium on Computer-Human Interaction in Play*, 2024, pp. 434–437.
- [9] D. M. Markowitz, R. Laha, B. P. Perone, R. D. Pea, and J. N. Bailenson, "Immersive virtual reality field trips facilitate learning about climate change," *Frontiers in psychology*, vol. 9, p. 2364, 2018.
- [10] P. Chapman, K. Bale, and P. Drap, "We all live in a virtual submarine," *IEEE Computer Graphics and Applications*, vol. 30, no. 1, pp. 85–89, 2010.
- [11] M. Haydar, D. Roussel, M. Maïdi, S. Otmane, and M. Mallem, "Virtual and augmented reality for cultural computing and heritage: a case study of virtual exploration of underwater archaeological sites (preprint)," *Virtual reality*, vol. 15, pp. 311–327, 2011.

- [12] Y. Wang, W. Zhang, Y. Chen, D. Liu, and H. Huang, "Study on underwater wet arc welding training with haptic device," in *2009 IEEE International Conference on Virtual Environments, Human-Computer Interfaces and Measurements Systems*. IEEE, 2009, pp. 191–195.
- [13] D. Hatushika, K. Nagata, and Y. Hashimoto, "Underwater vr experience system for scuba training using underwater wired hmd," in *OCEANS 2018 MTS/IEEE Charleston*, 2018, pp. 1–7.
- [14] C. Sinnott, J. Liu, C. Matera, S. Halow, A. Jones, M. Moroz, J. Mulligan, M. Crognale, E. Folmer, and P. MacNeilage, "Underwater virtual reality system for neutral buoyancy training: Development and evaluation," in *Proceedings of the 25th ACM Symposium on Virtual Reality Software and Technology*, 2019, pp. 1–9.
- [15] T.-P. G. Chen, Y. Kinoshita, Y. Takama, S. Fels, K. Funahashi, and A. Gadd, "Swimming across the pacific: A virtual swimming interface," in *ACM SIGGRAPH 2004 Emerging technologies*, 2004, p. 27.
- [16] D. Jain, M. Sra, J. Guo, R. Marques, R. Wu, J. Chiu, and C. Schmandt, "Immersive terrestrial scuba diving using virtual reality," in *Proceedings of the 2016 CHI Conference Extended Abstracts on Human Factors in Computing Systems*, ser. CHI EA '16. New York, NY, USA: Association for Computing Machinery, 2016, p. 1563–1569. [Online]. Available: <https://doi.org/10.1145/2851581.2892503>
- [17] L. Calvi, C. P. Santos, J. Relouw, B. Endrovski, C. Rothwell, A. Sarà, S. Lucrezi, M. Palma, and U. Pantaleo, "A vr game to teach underwater sustainability while diving," in *2017 Sustainable Internet and ICT for Sustainability (SustainIT)*, 2017, pp. 1–4.
- [18] Y. Dobashi, M. Sato, S. Hasegawa, T. Yamamoto, M. Kato, and T. Nishita, "A fluid resistance map method for real-time haptic interaction with fluids," in *Proceedings of the ACM symposium on Virtual reality software and technology*, 2006, pp. 91–99.
- [19] M. Yang, J. Lu, A. Safonova, and K. J. Kuchenbecker, "Gpu methods for real-time haptic interaction with 3d fluids," in *2009 IEEE International Workshop on Haptic Audio visual Environments and Games*. IEEE, 2009, pp. 24–29.
- [20] G. Cirio, M. Marchal, A. Lécuyer, and J. R. Cooperstock, "Vibrotactile rendering of splashing fluids," *IEEE Transactions on Haptics*, vol. 6, no. 1, pp. 117–122, 2013.
- [21] J. Jang and J. Park, "Sph fluid tactile rendering for ultrasonic mid-air haptics," *IEEE Transactions on Haptics*, vol. 13, no. 1, pp. 116–122, 2020.
- [22] M. Vines, J. Mora, and W.-S. Lee, "Haptic display of 3d liquids for interactive applications," in *2009 International IEEE Consumer Electronics Society's Games Innovations Conference*. IEEE, 2009, pp. 140–148.
- [23] E.-C. Lee, Y.-H. Cho, and I.-K. Lee, "Simulating water resistance in a virtual underwater experience using a visual motion delay effect," in *2019 IEEE Conference on Virtual Reality and 3D User Interfaces (VR)*, 2019, pp. 259–266.
- [24] H. Kang, G. Lee, and J. Han, "Visual manipulation for underwater drag force perception in immersive virtual environments," in *2019 IEEE Conference on Virtual Reality and 3D User Interfaces (VR)*, 2019, pp. 38–46.
- [25] A. Schmidt, A. Pereira, T. Baker, B. Pleintinger, T. Hulin, Z. Chen, D. A. Abbink, and N. Y. Lii, "Enabling interaction with virtual fluids and mixed media using a high dexterity hand exoskeleton," in *2020 IEEE International Conference on Systems, Man, and Cybernetics (SMC)*. IEEE, 2020, pp. 2925–2932.
- [26] R. Sawahashi, T. Masuda, T. Shimizu, R. Nishihama, M. Okui, and T. Nakamura, "Presentation of underwater sensation by drag in knee motion with a lower limb exoskeleton using mr fluid brakes," in *2023 IEEE 32nd International Symposium on Industrial Electronics (ISIE)*. IEEE, 2023, pp. 1–6.
- [27] T. Sarpkaya, "Vortex shedding and resistance in harmonic flow about smooth and rough circular cylinders," *BOSS-76*, vol. 1, pp. 220–235, 1976.
- [28] F. M. White, C. Ng, and S. Saimek, *Fluid mechanics*. McGraw-Hill, cop., 2011.
- [29] J. Mora and W.-S. Lee, "Real-time 3d fluid interaction with a haptic user interface," in *2008 IEEE Symposium on 3D User Interfaces*. IEEE, 2008, pp. 75–81.
- [30] B. Baxter and M. C. Lin, "Haptic interaction with fluid media." in *Graphics Interface*. Citeseer, 2004, pp. 81–88.
- [31] G. Cirio, M. Marchal, M. A. Otaduy, and A. Lécuyer, "Six-dof haptic interaction with fluids, solids, and their transitions," in *2013 World Haptics Conference (WHC)*, 2013, pp. 157–162.
- [32] J. Liang, G. Yu, K. Wang, Y. Wang, and L. Guo, "Realtime haptic rendering in hybrid environment using unified sph method," in *2016 3rd International Conference on Soft Computing & Machine Intelligence (ISCMi)*. IEEE, 2016, pp. 184–188.
- [33] H. Cheng and S. Liu, "Haptic force guided sound synthesis in multisensory virtual reality (vr) simulation for rigid-fluid interaction," in *2019 IEEE Conference on Virtual Reality and 3D User Interfaces (VR)*. IEEE, 2019, pp. 111–119.
- [34] P. Xia, "New advances for haptic rendering: state of the art," *The Visual Computer*, vol. 34, pp. 271–287, 2018.
- [35] L. Huang, S. Garbaya, and S. Khelladi, "Haptic interaction with fluids in virtual environment: an analytical review," *Virtual Reality*, vol. 29, no. 2, p. 62, 2025.
- [36] X. Zhang and S. Liu, "Sph haptic interaction with multiple-fluid simulation," *Virtual Reality*, vol. 21, pp. 165–175, 2017.
- [37] Z. Wang and Y. Wang, "Haptic interaction with fluid based on smooth particles and finite elements," in *Computational Science and Its Applications–ICCSA 2014: 14th International Conference, Guimarães, Portugal, June 30–July 3, 2014, Proceedings, Part I 14*. Springer, 2014, pp. 808–823.
- [38] H. Barreiro, S. Sinclair, and M. A. Otaduy, "Ultrasound rendering of tactile interaction with fluids," in *2019 IEEE World Haptics Conference (WHC)*, 2019, pp. 521–526.
- [39] P. Ratsamee, Y. Orita, Y. Kuroda, and H. Takemura, "Flowhaptics: Mid-air haptic representation of liquid flow," *Applied Sciences*, vol. 11, no. 18, p. 8447, 2021.
- [40] L. Liu, C. Yao, Y. Liu, P. Wang, Y. Chen, and F. Ying, *FlowGlove: A Liquid-Based Wearable Device for Haptic Interaction in Virtual Reality*, 11 2020, pp. 316–331.
- [41] D. Ryu, G.-H. Yang, and S. Kang, "T-hive: Vibrotactile interface presenting spatial information on handle surface," in *2009 IEEE International Conference on Robotics and Automation*. IEEE, 2009, pp. 683–688.
- [42] E. Piateski and L. Jones, "Vibrotactile pattern recognition on the arm and torso," in *First Joint Eurohaptics Conference and Symposium on Haptic Interfaces for Virtual Environment and Teleoperator Systems. World Haptics Conference*. IEEE, 2005, pp. 90–95.
- [43] G. Huisman, A. D. Frederiks, B. Van Dijk, D. Hevlen, and B. Kröse, "The tasst: Tactile sleeve for social touch," in *2013 World Haptics Conference (WHC)*. IEEE, 2013, pp. 211–216.
- [44] H. Culbertson, C. M. Nunez, A. Israr, F. Lau, F. Abnousi, and A. M. Okamura, "A social haptic device to create continuous lateral motion using sequential normal indentation," in *2018 IEEE Haptics Symposium (HAPTICS)*. IEEE, 2018, pp. 32–39.
- [45] W. Wu and H. Culbertson, "Wearable haptic pneumatic device for creating the illusion of lateral motion on the arm," in *2019 IEEE World Haptics Conference (WHC)*. IEEE, 2019, pp. 193–198.
- [46] J. Park, J. Kim, Y. Oh, and H. Z. Tan, "Rendering moving tactile stroke on the palm using a sparse 2d array," in *Haptics: Perception, Devices, Control, and Applications: 10th International Conference, EuroHaptics 2016, London, UK, July 4–7, 2016, Proceedings, Part I 10*. Springer, 2016, pp. 47–56.
- [47] Y. Ma, T. Xie, P. Zhang, H. Kim, and S. Je, "Airpush: A pneumatic wearable haptic device providing multi-dimensional force feedback on a fingertip," in *Proceedings of the CHI Conference on Human Factors in Computing Systems*, 2024, pp. 1–13.
- [48] I. Jo, Y. Park, H. Kim, and J. Bae, "Evaluation of a wearable hand kinesthetic feedback system for virtual reality: psychophysical and user experience evaluation," *IEEE Transactions on Human-Machine Systems*, vol. 49, no. 5, pp. 430–439, 2019.
- [49] M. Bilinauskaitė, V. R. Mantha, A. I. Rouboa, P. Ziliukas, A. J. Silva et al., "Computational fluid dynamics study of swimmer's hand velocity, orientation, and shape: contributions to hydrodynamics," *BioMed research international*, vol. 2013, 2013.
- [50] J. Berg, R. Bazuin, C. Jux, A. Sciacchitano, J. Westerweel, and W. Water, "The effect of hand posture on swimming efficiency," *Experiments in Fluids*, vol. 62, 12 2021.
- [51] S. A. Thorpe et al., *An introduction to ocean turbulence*. Cambridge University Press Cambridge, 2007, vol. 10.
- [52] S. Derler and L.-C. Gerhardt, "Tribology of skin: review and analysis of experimental results for the friction coefficient of human skin," *Tribology Letters*, vol. 45, pp. 1–27, 2012.
- [53] B. Voisin, "Added mass of oscillating bodies in stratified fluids," *Journal of Fluid Mechanics*, vol. 987, p. A27, 2024.
- [54] H. Schlichting and K. Gersten, *Boundary-layer theory*. Springer, 2016.
- [55] M. W. Uddin, X. Zhang, and D. Wang, "A pneumatic-driven haptic glove with force and tactile feedback," in *2016 International Conference on Virtual Reality and Visualization (ICVRV)*. IEEE, 2016, pp. 304–311.
- [56] S. F. Hoerner, "Fluid-dynamic drag." *CHAPTER V-Drag of Surface Imperfections*, 1958.

- [57] M. Tavallaeinejad, M. P. Paidoussis, and M. Legrand, "Nonlinear static response of low-aspect-ratio inverted flags subjected to a steady flow," *Journal of Fluids and Structures*, vol. 83, pp. 413–428, 2018. [Online]. Available: <https://www.sciencedirect.com/science/article/pii/S0889974618301749>
- [58] W. Bollay, "A non-linear wing theory and its application to rectangular wings of small aspect ratio," *ZAMM-Journal of Applied Mathematics and Mechanics/Zeitschrift für Angewandte Mathematik und Mechanik*, vol. 19, no. 1, pp. 21–35, 1939.
- [59] I. Cheeseman, "Fluid-dynamic drag: Practical information on aerodynamic drag and hydrodynamic resistance. sf hoerner. hoerner fluid dynamics, brick town, new jersey. 1965. 455 pp. illustrated." *The Aeronautical Journal*, vol. 80, no. 788, pp. 371–371, 1976.
- [60] E.-S. Aziz, C. Chassapis, S. Esche, S. Dai, S. Xu, and R. Jia, "Online wind tunnel laboratory," in *2008 Annual Conference & Exposition*, 2008, pp. 13–949.
- [61] G. Schewe, "Reynolds-number-effects in flow around a rectangular cylinder with aspect ratio 1: 5," *Journal of Fluids and Structures*, vol. 39, pp. 15–26, 2013.
- [62] T. M. Greiner, *Hand anthropometry of US army personnel*. US Army Natick Research, Development & Engineering Center Natick, MA, 1991.
- [63] A. E. Minetti, G. Machtiras, and J. C. Masters, "The optimum finger spacing in human swimming," *Journal of biomechanics*, vol. 42, no. 13, pp. 2188–2190, 2009.
- [64] Y. Huang, K. Yao, J. Li, D. Li, H. Jia, Y. Liu, C. K. Yiu, W. Park, and X. Yu, "Recent advances in multi-mode haptic feedback technologies towards wearable interfaces," *Materials Today Physics*, vol. 22, p. 100602, 2022.
- [65] G. Chen, M. M. Alam, and Y. Zhou, "Dependence of added mass on cylinder cross-sectional geometry and orientation," *Journal of Fluids and Structures*, vol. 99, p. 103142, 2020.
- [66] D. Koga, T. Tsunokawa, Y. Sengoku, K. Homoto, Y. Nakazono, and H. Takagi, "Relationship between hand kinematics, hand hydrodynamic pressure distribution and hand propulsive force in sprint front crawl swimming," *Frontiers in Sports and Active Living*, vol. 4, p. 786459, 2022.
- [67] P. Morasso, "Spatial control of arm movements," *Experimental brain research*, vol. 42, no. 2, pp. 223–227, 1981.
- [68] C. G. Atkeson and J. M. Hollerbach, "Kinematic features of unrestrained vertical arm movements," *Journal of Neuroscience*, vol. 5, no. 9, pp. 2318–2330, 1985.
- [69] M. Kücken, "Models for fingerprint pattern formation," *Forensic science international*, vol. 171, no. 2-3, pp. 85–96, 2007.
- [70] K. Myles and M. S. Binseel, "The tactile modality: a review of tactile sensitivity and human tactile interfaces," *US Army Research Laboratory, ARL-TR-4115, Aberdeen Proving Ground, MD*, vol. 21005, p. 5425, 2007.
- [71] H. Luo, Z. Wang, Z. Wang, Y. Zhang, and D. Wang, "Perceptual localization performance of the whole hand vibrotactile funneling illusion," *IEEE Transactions on Haptics*, 2023.
- [72] HaptX, "HaptX dk2," <https://haptx.com/>, 2021.
- [73] Y. Semenov, Y. Savchenko, and G. Savchenko, "Impulsive impact of a submerged body," *Journal of Fluid Mechanics*, vol. 919, p. R4, 2021.
- [74] S. Chaudhuri and A. Bhardwaj, "Kinesthetic perception," *A Machine Learning Approach*, 2018.
- [75] C.-Y. Tsai, I.-L. Tsai, C.-J. Lai, D. Chow, L. Wei, L.-P. Cheng, and M. Y. Chen, "Airracket: Perceptual design of ungrounded, directional force feedback to improve virtual racket sports experiences," in *Proceedings of the 2022 CHI Conference on Human Factors in Computing Systems*, 2022, pp. 1–15.
- [76] J. Kim, S. Oh, C. Park, and S. Choi, "Body-penetrating tactile phantom sensations," in *Proceedings of the 2020 CHI Conference on Human Factors in Computing Systems*, 2020, pp. 1–13.
- [77] M. Elgendi, F. Picón, and N. Magenant-Thalmann, "Real-time speed detection of hand gesture using kinect," in *Proc. Workshop on Autonomous Social Robots and Virtual Humans, The 25th Annual Conference on Computer Animation and Social Agents (CASA 2012)*, 2012, pp. 1–15.
- [78] Z. Cai and M. Wiertlewski, "Ultraloop: Active lateral force feedback using resonant traveling waves," *IEEE Transactions on Haptics*, 2023.
- [79] C. Papaxanthis, T. Pozzo, and M. Schieppati, "Trajectories of arm pointing movements on the sagittal plane vary with both direction and speed," *Experimental brain research*, vol. 148, pp. 498–503, 2003.
- [80] J. P. Rodrigues, F. L. Mastaglia, and G. W. Thickbroom, "Rapid slowing of maximal finger movement rate: fatigue of central motor control?" *Experimental brain research*, vol. 196, pp. 557–563, 2009.
- [81] K. Salisbury, F. Conti, and F. Barbagli, "Haptic rendering: introductory concepts," *IEEE computer graphics and applications*, vol. 24, no. 2, pp. 24–32, 2004.
- [82] K. Salisbury, D. Brock, T. Massie, N. Swarup, and C. Zilles, "Haptic rendering: Programming touch interaction with virtual objects," in *Proceedings of the 1995 symposium on Interactive 3D graphics*, 1995, pp. 123–130.
- [83] S. Cobos, M. Ferre, M. S. Uran, J. Ortego, and C. Pena, "Efficient human hand kinematics for manipulation tasks," in *2008 IEEE/RSJ International Conference on Intelligent Robots and Systems*. IEEE, 2008, pp. 2246–2251.
- [84] B. G. Witmer and M. J. Singer, "Measuring presence in virtual environments: A presence questionnaire," *Presence*, vol. 7, no. 3, pp. 225–240, 1998.
- [85] Y.-H. Lin, Y.-W. Wang, P.-S. Ku, Y.-T. Cheng, Y.-C. Hsu, C.-Y. Tsai, and M. Y. Chen, "Hapticsense: a multi-channel, black-box, platform-agnostic approach to detecting video game events for real-time haptic feedback," in *Proceedings of the 2021 CHI conference on human factors in computing systems*, 2021, pp. 1–14.
- [86] V. Shen, T. Rae-Grant, J. Mullenbach, C. Harrison, and C. Shultz, "Fluid reality: High-resolution, untethered haptic gloves using electroosmotic pump arrays," in *Proceedings of the 36th Annual ACM Symposium on User Interface Software and Technology*, 2023, pp. 1–20.
- [87] J. Hartcher-O'Brien, V. Mehta, N. Colonnese, A. Gupta, C. J. Bruns, P. Agarwal et al., "Fingertip wearable high-resolution electrohydraulic interface for multimodal haptics," in *2023 IEEE World Haptics Conference (WHC)*. IEEE, 2023, pp. 299–305.
- [88] W. M. B. Tiest, N. D. Kosters, A. M. Kappers, and H. A. Daanen, "Haptic perception of wetness," *Acta psychologica*, vol. 141, no. 2, pp. 159–163, 2012.
- [89] D. Filingeri, D. Fournet, S. Hodder, and G. Havenith, "Why wet feels wet? a neurophysiological model of human cutaneous wetness sensitivity," *Journal of neurophysiology*, vol. 112, no. 6, pp. 1457–1469, 2014.
- [90] Y.-Y. Liao, Y.-F. Hong, P.-H. Han, and J.-C. Ko, "Liquidmask: utilizing liquid-based haptic for multiple tactile sensation in immersive virtual reality," in *ACM SIGGRAPH 2019 Virtual, Augmented, and Mixed Reality*, 2019, pp. 1–1.
- [91] S.-H. Liu, P.-C. Yen, Y.-H. Mao, Y.-H. Lin, E. Chandra, and M. Y. Chen, "Headblaster: a wearable approach to simulating motion perception using head-mounted air propulsion jets," *ACM Transactions On Graphics (TOG)*, vol. 39, no. 4, pp. 84–1, 2020.



Soyeong Yang is a Ph.D. student in the HCI Tech Lab at the Korea Advanced Institute of Science and Technology (KAIST). Her research focuses on haptic rendering, human perception, and virtual reality, with an emphasis on developing algorithms that enable haptic feedback to provide perceptually rich and cognitively meaningful experiences in VR. She received her B.S. degree in Computer Art from Chung-Ang University and her M.S. degree from the Graduate School of Metaverse and Culture Technology at KAIST.



Sang Ho Yoon is an associate professor in the Graduate School of Culture Technology at the Korea Advanced Institute of Science and Technology (KAIST), with a joint appointment at the School of Computing, the Graduate School of Metaverse, and the Robotics Program. He leads the HCI Tech Lab. His research focuses on developing natural user interactions that address physical, mental, and social barriers with novel haptic interfaces and sensing techniques. He received his Ph.D. in Mechanical Engineering from Purdue University and his B.S. and M.S. degrees in Mechanical Engineering from Carnegie Mellon University.